DKK1 AS A NOVEL CANDIDATE THERAPEUTIC TARGET OF GLIOBLASTOMA

IDENTIFICATION AND VALIDATION OF DKK1 AS A NOVEL CANDIDATE

THERAPEUTIC TARGET FOR GLIOBLASTOMA

By NICOLAS YELLE, B.Sc.

A Thesis Submitted to the School of Graduate Studies in Partial Fulfilment of the

Requirements for the degree Master of Science

McMaster University MASTER OF SCIENCE (2018) Hamilton, Ontario (Biochemistry)

TITLE: Identification and Validation of DKK1 as a novel marker of glioblastoma

AUTHOR: Nicolas Yelle, B.Sc. (McMaster University) SUPERVISOR: Professor Sheila

K. Singh NUMBER OF PAGES: xvii, 84

LAY ABSTRACT

Glioblastoma (GBM) is an aggressive tumour that relapses within nine months of diagnosis and remains incurable despite chemotherapy, radiation, and surgery. Relapse is believed to be caused by the presence of a wide variety of cell types, including cancer stem cells (CSCs), which have been shown to be resistant to both chemotherapy and radiation. As a result, therapies that focus on targeting the CSCs within GBM would provide better treatment. In this study, we analyzed this cell population by conducting two screens. The first compared gene expression levels in GBM CSCs to their healthy counterparts, neural stem cells, whereas the second compared the primary patient GBM tumour to its relapsed form in a mouse model of the disease. In this study, the protein Dickkopf-1 (DKK1) was identified and validated as a potential therapeutic target of GBM using well established molecular and stem cell functional assays.

ABSTRACT

Glioblastoma (GBM) is a very aggressive and invasive tumour that relapses within nine months of diagnosis and remains incurable despite advances in multimodal therapy including surgical resection, chemotherapy and radiation. Poor patient outcome has been correlated to specific markers of brain tumour initiating cells (BTIC) and intratumoural heterogeneity (ITH), which have also been associated with treatment resistance and tumour recurrence. ITH can be explained at the cellular level by the existence of multiple populations of cancer cells, including some which have acquired stemness properties like self-renewal, proliferation, and multilineage differentiation, also known as cancer stem cells (CSCs). In brain tumours, CSCs or BTICs, have been shown to be resistant to both chemotherapy and radiation treatment, allowing them to escape therapy and consequently generate for tumour recurrence. As a result, therapies that focus on targeting the BTIC compartment within the bulk GBM tumour would provide better treatment and prognosis for patients. To profile GBM BTICs we conducted two transcriptomic screens. The first compared GBM BTICs to neural stem cells (NSCs), their healthy counterparts, and for the second we developed a pipeline utilizing a dynamic BTIC patient-derived xenograft (PDX) model of human GBM recurrence allowing for the profiling of GBM BTICs at engraftment, after chemoradiotherapy delivery in a phase we have termed "minimal residual disease" (MRD), and at tumour recurrence. In this study, Dickkopf-1 (DKK1) was identified as a potential therapeutic target for GBM from each transcriptomic screen and was studied using

short hairpin knockdowns, blockade with monoclonal antibodies, and subsequent functional stem cell assays.

ACKNOWLEDGEMENTS

years. Finally, a very, very special thanks to my parents who made me who I am today, and who without I would not be here. And thank you to Michelle Ly for always being there for me – even after leaving me for Toronto – and for her constant love and support, and whom without I would have procrastinated even more than I already did in writing this thesis.

TABLE OF CONTENTS

LIST OF FIGURES

LIST OF TABLES

Table 1. Top hits of differentially expressed genes in CD133+ compared to CD133- glioblastoma populations.

Table 2. Top hits of differentially expressed genes in CD133+ compared to CD133- neural stem and progenitor cell populations.

Table 3. Top hits of differentially expressed genes in CD133+ glioblastoma compared to CD133+ neural stem and progenitor cell populations.

Table 4. Top hits of differentially expressed genes in CD133- glioblastoma compared to CD133- neural stem and progenitor cell populations.

Table 5. Refined list of top-12 candidate targets of glioblastoma.

ABBREVIATIONS AND SYMBOLS

Akt	Protein kinase B; PKB
APC	Adenomatous polyposis coli
Bmi1	Polycomb complex protein BMI-1
BTIC	Brain tumour initiating cells
BiTEs	Bi-specific T cell engagers
BsAb	Bi-specific monoclonal antibody
CAR	Chimeric antigen receptor
CCAB	Centre for the Commercialization of Antibiotics and Biologics
CEA	Carcinoembryonic antigen
CKAP4	Cytoskeleton associated protein 4
CKIa	Casein Kinase I alpha
CSC	Cancer stem cells
CT	Computed tomography
DKK1	Dickkopf-1
DKK2	Dickkopf-2
DKK3	Dickkopf-3
DKK4	Dickkopf-4
EDTA	Ethylenediaminetetraacetic acid
EGFR	Epidermal growth factor receptor
EGFRvIII	Epidermal growth factor receptor, variant III

EpCAM	Epithelial cell adhesion molecule
EphA2	Ephrin receptor A2
EphA3	Ephrin receptor A3
EphB2	Ephrin receptor B2
FACS	Fluorescence activated cell sorting
FC	Fold-change
FDA	Federal Drug Administration of the USA
FoxG1	Forkhead box G1
FZD	Frizzled receptor
GBM	Glioblastoma
rGBM	Recurrent glioblastoma
GSK3	Glycogen Synthase Kinase 3
Gy	Gray (unit)
H&E	Hematoxylin and eosin
IDH1	Isocitrate dehydrogenase 1
IgG	Immunoglobulin G
ITGA6	Integrin alpha-6
ITH	Intratumoural heterogeneity
IV	Intravenous
IVIS	In Vivo Imaging System
JNK	c-Jun N-terminal kinase
K_D	Dissociation constant

Krm1/2	Kremen-1/2
LCC	Latency competent cancer
LRP5/6	Low-density lipoprotein receptor-related protein 5 and 6
L1CAM	L1 cell adhesion molecule
mAb	Monoclonal antibody
MAPK	Mitogen-activated protein kinase
MDSC	Myeloid derived suppressor cells
MHC 1	Major histocompatibility complex type 1
MRD	Minimal residual disease
MRI	Magnetic Resonance Imaging
NEFL	Neurofilament light
NF1	Neurofibromin 1
NK	Natural killer
NSC	Neural stem cells
NSPC	Neural stem and progenitor cells
NSG	NOD SCID gamma
Oct4	Octamer-binding transcription factor 4
PDGFRA	Platelet-derived growth factor receptor A
PDL	Patient-derived line
PDX	Patient-derived xenograft
PE	Phycoerythrin
PI3K	Phosphoinositide 3-kinase

PROM1	Prominin-1; CD133
PSMA	Prostate-specific membrane antigen
RBC	Red blood cells
RNA	Ribonucleic acid
RNA-Seq	Ribonucleic acid sequencing
ROR	Receptor tyrosine kinase-like orphan receptor
RT-qPCR	Reverse transcriptase quantitative polymerase chain reaction
RTK	Receptor tyrosine kinase
RYK	Related to receptor tyrosine kinase
scFv	Single-chain variable fragment
shDKK1	shRNA targeting DKK1
shRNA	Short-hairpin ribonucleic acid
Sox2	Sex-determining region Y (SRY)-box 2
SLC12A5	Solute carrier family 12 member 5
SYT1	Synaptotagmin 1
TCF/LEF	T-cell factor/lymphoid enhancing factors
TCGA	The Cancer Genome Atlas
TCR	T cell receptor
TMZ	Temozolomide
TP53	Tumour protein p53
TRAC	Toronto Recombinant Antibody Centre
WHO	World Health Organization

DECLARATION OF ACADEMIC ACHIEVEMENT

This project was supervised by Dr. Sheila Singh. She, along with Dr. Chitra Venugopal and Dr. Parvez Vora participated in the designing of experiments. Dr. Mohini Singh participated in the injection of GBM patient-derived cells. Dr. Kevin Brown of Dr. Jason Moffat's laboratory performed the bioinformatics analyses relating to the recurrent GBM RNA-Seq analyses (Project 1). Dr. Jeff Liu of Dr. Gary Bader's laboratory performed the bioinformatics analyses relating to the GBM BTIC RNA-Seq analysis (Project 2). Chirayu Chokshi participated in the optimization of the patient-derived xenograft (PDX) treatment regimen and the treatment of the PDXs. Dr. Kim Desmond of Dr. Nicholas Bock's laboratory participated by conducting all of the MRI scans. Minomi Subapanditha participated in everything relating to flow cytometry. I contributed to the design and execution of the experiments presented, performed data analyses, and writing of all sections in this thesis unless otherwise stated.

INTRODUCTION

Clinical relevance of glioblastoma

Glioblastoma (GBM) is the most common and aggressive adult primary brain tumour, feared for its uniformly fatal prognosis. Common treatment for GBM consists of multimodal therapy including of surgical resectioning followed by chemotherapy and radiation therapy. Unfortunately, even after the addition of the chemotherapeutic drug temozolomide (TMZ) to their treatment regimens, patients on average experience relapse 9 months post-diagnosis with the median survival being approximately 15 months, and less than 10% surviving over two years without relapsing (Ohgaki H, 2005; Louis DN e. a., 2007; Stupp R, 2005; Pastrana E, 2011). As GBM remains incurable, and treatment abysmal, there is an urgent need to identify new therapeutics that can improve GBM patient outcome.

GBM is the most aggressive type of astrocytoma, designated as a grade IV astrocytoma by the World Health Organization (WHO) (Louis DN, 2016). As their name suggests, astrocytomas are cancers of the astrocytes, which are star-shaped glial cells in the brain that perform many functions including the support of endothelial cells forming the blood brain barrier, provision of nutrients for the nervous tissue, and repair and healing. Astrocytomas can develop at any age (peak incidence between the ages of 45 and 75) and can be difficult to diagnose, as symptoms not only aren't definitive, but they don't always

manifest until very late in the tumour's progression. As astrocytomas can occur in any part of the brain, their symptoms depend on the tumour's location and include seizures, nausea, headaches, vomiting, hemiparesis (weakness of the right or left side of the body), as well as memory, personality, and neurological deficits. Diagnosis of astrocytomas is done with computed tomography (CT) scan, or magnetic resonance imaging (MRI) to properly characterize the tumour size and location, before a biopsy of the tumour is performed and then graded. Biopsies can occur before or during surgical resection. Astrocytoma grading, consisting of four grades, was established in 1993 by the WHO based on histological characteristics (i.e. atypia, mitosis, endothelial and vasculature proliferation, necrosis) of the tumour in order to eliminate confusion in diagnosis (Verhaak R, 2010). WHO grade I astrocytomas do not display any of the aforementioned histological characteristics, are slow-growing, benign, and are associated with long-term survival and possible complete remission. WHO grade II astrocytomas display one of the histological characteristics, are slow-growing but can be invasive, have the possibility of recurring and evolving into a higher-grade tumour, and are associated with a median survival of 4 years. WHO grade III astrocytomas display two of the histological characteristics, are anaplastic, invasive, recurrent, have a median survival of 18 months without treatment, and are associated with a 5-year survival rate of 24%. WHO grade IV astrocytomas (GBM) display 3 or more of the histological characteristics and are essentially a more extreme version of the grade III astrocytomas. They are characterized by necrotizing tissue, hyperplastic blood vessels, and are anaplastic, fast-growing, extremely invasive, such that recurrence is inevitable (Louis

2

DN, 2016). The median survival for a GBM patient is 15 months, with about a quarter of patients surviving for up to two years (Stupp R, 2005).

Intratumoural heterogeneity

Like all tumours, GBM is not made up of a homogenous population of cells as was once believed. GBMs have been known to be extensively heterogeneous in every way including on the patient, intratumoural, cellular, and genetic levels. It is this heterogeneity that has been attributed to treatment failure and tumour relapse (Wechsler-Reya R, 2001; Zhu Y, 2002; Huse JT, 2010). In a study lead by Verhaak and colleagues at The Cancer Genome Atlas Research Network (TCGA), four genetic subtypes of GBM were identified by bulk-tumour sequencing: classical, proneural, neural, and mesenchymal (Verhaak R, 2010). The classical subtype was characterized by extra copies and an overexpression of the EGFR (epidermal growth factor receptor) gene, with the TP53 (p53) gene largely remaining not mutated. The proneural subtype was characterized by mutations in IDH1 (isocitrate dehydrogenase), TP53, and PDGFRA (platelet-derived growth factor receptor). The neural subtype was characterized by the expression of neuron markers such as NEFL, GABRA1, SYT1, and SLC12A5. The mesenchymal subtype was characterized by mutations in the NF1 (neurofibromin 1), and a low-rate of mutations and an underexpression of EGFR.

However, some recent studies have put into question the GBM subtypes, demonstrating additional genetic and spatial heterogeneity. Szerlip and colleagues first

3

demonstrated that receptor tyrosine kinases (RTKs), namely EGFR and PDGFRA, were amplified in a heterogeneous manner in GBM subpopulations (Szerlip NJ, 2012). Sottoriva and colleagues then demonstrated GBM spatial intratumour heterogeneity by analyzing the genetic expression of tumour fragments from the same tumour and classifying them under different GBM subtypes (Sottoriva A, 2013). Patel and colleagues reinforced the prior studies by applying single-cell RNA-Seq to demonstrate that a GBM tumour is actually made up of a mixture of different cells that can be classified in each of the subtypes (Patel AP, 2014). These studies successfully demonstrate the extensive heterogeneous nature of GBMs.

Clonal evolution and therapy resistance

The fact that GBMs are made up of many different populations leads to many clinical issues involving recurrence and treatment resistance (Burrell R, 2013; Swanton, 2015; Meacham CE, 2013). The presence of many subpopulations within each GBM would help partially explain both latter phenomena, as therapy has been shown to give rise to subclonal populations with selected traits enabling them to escape therapy (Notta F, 2011). Additional recent studies have corroborated this as GBM subclonal populations were shown to have distinct genetic identities and have variable drug-resistance profiles and responses to TMZ (Meyer M, 2015; Reinartz R, 2017). Johnson and colleagues demonstrated that primary gliomas and their paired recurrent tumours are highly divergent and only share a few mutations in common. In almost half of the cases studied, over half

of the mutations were no longer detectable at recurrence (Johnson BE, 2014). More recent studies have shown that driver clonal mutations in the primary GBM are often lost in recurrence, which are largely driven by subclonal populations bearing mutations not present in the primary GBM (Kim H, 2015; Favero, 2015). Another study went even further and demonstrated that spatially local recurrences bear a number of the initial tumour's mutations, then go on to follow a linear evolution model leading to decreased retained mutations in more spatially distant locations (Kim J, 2015).

Altogether, these studies point to therapy acting as a strong selection pressure allowing for treatment-resistant clones to emerge and drive GBM recurrence. Similar to an antibiotic-resistant superbug, recurrence seems to be driven by the remaining treatment-resistant population. Conventional therapy acts as a bottleneck for tumour subclonal evolution by killing off the non-resistant tumour cells, leaving behind only the resistant clones, resulting in remission. Thus when the tumour recurs, it is resistant to conventional therapy in the same way superbugs are resistant to widely used antibiotics. These are some of the reasons many believe a "cure-all magic-bullet" isn't possible in cancer therapy, and that monotherapies are doomed to fail (Ramaswamy V, 2015; Scorsetti M, 2015; Wei W, 2016).

Cancer Stem Cells and Brain Tumour Initiating Cells

While studying cancer heterogeneity, it was discovered that not all cancer cells are equal in their abilities to proliferate, self-renew, and maintain the tumour

microenvironment. Bonnet and Dick discovered what are now known as leukemia cancer stem cells (CSC), sparking the birth of the cancer stem cell hypothesis (Bonnet D, 1997). According to the theory, a small population of cells within a tumour, the CSCs, exhibits many stem cell qualities such as the ability to self-renew, proliferate, enter senescence, and of multilineage differentiation. It is believed that these cells give rise to the tumour heterogeneity, and therefore contribute directly to ITH and treatment resistance. The first solid tumour CSCs were discovered by Al Hajj in breast cancer (Al Hajj M, 2003). Brain tumours CSCs, also known as brain tumour initiating cells (BTICs), were discovered based on the established neural stem cell marker, prominin-1 (PROM1) also known as CD133 (Singh SK, 2004; Singh SK, 2003; Uchida N, 2000). BTIC subpopulations have since been studied and identified based on CD133 (Singh SK, 2004), CD15 (Son MJ, 2009), ITGA6 (Lathia JD, 2010), L1CAM (Bao S, 2008), EphA2 (Binda E, 2012), EphA3 (Day BW, 2013), EphB2 (Nakada M, 2010) Sox2 (Graham V, 2003), Msi1 (Kaneko Y, 2000), and Oct4 (Suva ML, 2014). Other genes such as FoxG1 (Manoranjan B, 2013) and Bmi1 (Fasano CA, 2007; Abdouh M, 2009) are important in preserving the stem cell state of BTICs.

In addition to being associated with ITH, BTICs have been shown to be resistant to chemotherapy (Murat A, 2008; Liu G, 2006; Beier D, 2012; Chen J, 2012) and radiation (Bao S, 2006), and have been shown to correlate with patient survival (Venugopal C, 2012). It has become apparent that in order to fully eradicate GBM from a patient, the BTIC subpopulations and their abilities to avoid therapy and to cause recurrence must be

addressed. A recent study done in the Singh lab has identified pyrvinium as a compound able to target the CD133+ human BTICs (Venugopal C, 2015).

Immunotherapy for glioblastoma

Immunotherapy has recently emerged as an attractive alternative to conventional therapy. Since GBM, and other solid tumours are very heterogeneous, many have long believed the key to cancer therapy will be found by tailoring regimens to every patient. As immunotherapy uses the host's immune system to target the disease, many remain optimistic in the search for a cure. Some of the most common antibody-based modalities are monoclonal antibodies (mAb), bi-specific antibodies (bsAb), bi-specific T cell engagers (BiTEs), and chimeric antigen receptor (CAR) T cells. mAbs can be used to bind to its epitope of interest and physically hinder its function, inhibit its downstream activities, or opsonize the target cell. The IV-injection of mAbs in pre-clinical and clinical trials of GBM has been shown to lead to therapeutic benefit on multiple occasions (Bourdon MA, 1984; Scott AM, 2007; Zalutsky MR, 1989). Anti-EGFR (Sym004; NCT02540161), anti-VEGF (bevacizumab; NCT01149850), anti-PSMA (89Zr-J591; NCT02410577), and anti-PDGFRA (Olaratumab; NCT00895180) mAbs are currently in phase II clinical trials.

BiTEs are a type of bi-specific antibody meant to direct the host's T cells cytotoxic activity to a target, which in this case is a cancerous cell. BiTEs are fusion proteins made up of two single-chain variable fragments (scFv), where one will bind to the CD3 receptor of a T cell, and the other to a cancer-related antigen. BiTEs can trigger apoptosis in a

tumour cell by activating T cells independently of major histocompatibility complex 1 (MHC I), by binding to both the former and the latter, leading to the formation of a synapse and by the release of perforins and granzymes. BiTEs specific for CD19 (blinatumomab) have shown to have remarkable potential in the treatment of B cell malignancies, and are also currently undergoing clinical investigations. BiTEs targeting other targets such as EpCAM, CEA, and PSMA are being used to treat solid tumours including colorectal, breast, ovarian, gastrointestinal, and prostate cancer (Suryadevara CM, 2015). In GBM, CD3/EGFR (Zitron IM, 2013) and CD3/EGFRvIII (Choi BD, 2013; Gedeon PC, 2014) BiTEs have also shown to be successful in pre-clinical models of GBM.

CARs are engineered T cell receptors (TCR) enabling the T cells to bind and target an epitope of choice. CARs are made up of a scFv from a mAb fused to a CD3-ζ transmembrane domain and an endodomain, which work to send an activation signal to the T cell after recognition of the target by the scFv. An advantage of CAR T cells is their ability to bypass the formation of the TCR:MHC complex needed in normal T cell activation. This is particularly important in GBM, as MHC I has been shown to be often downregulated in invasive glioma cells (Zagzag D, 2005). CAR T cells have garnered a significant amount of attention as of late due to unprecedented success in the treatment of haematological malignancies, targeting either CD19 or CD20 (Porter DL, 2011; Maude SL, 2014; Till BG, 2012; Kochenderfer JN, 2015). Since then, many have been applying CAR T cells to solid tumours, including GBM, where CAR T cells have been successful in pre-clinical models of the disease, typically targeting either EGFRvIII (Bullain SS, 2009; Morgan RA, 2012; Johnson LA, 2015; Miao H, 2014), or IL-13R (Kong S, 2012). A study

by Sampson and colleagues has additionally shown CAR T cells have the ability of killing GBM and inducing immunological memory in mice (Sampson JH, 2014). Finally, CAR T cells targeting EGFRvIII (NCT01454596), IL-13Rα2 (NCT02208362), and Her2 (NCT01109095) are currently under clinical investigation.

Secreted Wnt modulator DKK1 in cancer

The Wnt pathway is well-known and has been associated with a number of cellular processes including stem cell maintenance, cell fate decisions, proliferation, survival, migration, cell polarity, development and homeostasis (Sedgwick AE, 2016). The pathway is highly complex and includes 19 known Wnt ligands and 10 Frizzled receptors (FZD). Wnt activity can be divided into two pathways, β-catenin-dependent pathway (canonical Wnt pathway), and the β-catenin-independent pathway (noncanonical Wnt pathway). As is often the case with pathways associated with a number of essential roles, a number of mutations and dysregulations have been associated with many aspects of many cancers. Dickkopf-1 (DKK1) is a secreted Wnt modulator best known for directly inhibiting canonical Wnt by binding onto LRP5/6 and inducing conformational changes blocking all Wnt binding sites (Ahn VE, 2011; Bourhis E, 2011; Chen S, 2011; Cheng Z, 2011; Bao J, 2012; Matoba K, 2017). The binding of Wnt to LRP5/6 and FZD is needed for the activation of the pathway by stopping the phosphorylation and degradation of β-catenin by the destruction complex, made up of Axin, APC, CKIa, and GSK3 among others. When the pathway is activated, β-catenin accumulates in the cytoplasm and translocates to the

nucleus where it will interact with members of the T-cell factor/lymphoid enhancing factors (TCF/LEF) transcription factors to activate the Wnt transcriptional program. Although it isn't fully understood, activation of the β-catenin-independent pathway is thought to happen through the accumulation of Wnt which is no longer able to bind LRP5/6 because of DKK1, allowing it to bind ROR/RYK to activate it (Green J, 2014). Finally, DKK1 has more recently been shown to be able to activate PI3K/Akt through an interaction with CKAP4 (Kimura H, 2016).

DKK1 is the most well-known and studied member of the Dickkopf family of proteins, consisting of four members (DKK1-4). All members of the family are extremely context- and cancer-type-dependent and have each been shown to be either upregulated or downregulated in a wide variety of cancers (Shao YC, 2017). DKK2 has been shown to be both an agonist and antagonist of canonical Wnt, depending on cellular context and Krm2 (Mao B, 2003). DKK3 is the least studied of the Dickkopf family. Its role remains unclear and its influence on canonical Wnt signalling remains in question (Mohammadpour H, 2016; Nakamura RE, 2010). DKK4's role is very similar to DKK1's as they both bind LRP5/6 and Krm1/2 to antagonize canonical Wnt, but it is additionally thought to be able to signal through the MAPK and JNK pathways in pancreatic and renal cancer, respectively (Hirata H, 2009; Ouyang Y, 2016).

As alluded to, DKK1 plays an interesting and highly context-dependent role in cancer. Initially described as a canonical Wnt inhibitor, it was naturally thought to be a tumour suppressor as Wnt is widely seen as tumorigenic. However, DKK1 has been shown to be highly context-dependent and can act as a cancer promoter as well as a suppressor.

DKK1 has been shown to be decreased, silenced, or enhanced in a number of cancers, and has also been shown to decrease tumour proliferation, angiogenesis, invasion, and it has paradoxically also been shown to increase all of the above as well (Mazon M, 2016; Kagey MH, 2017). DKK1's function is likely not fully understood, and highly dependent on many factors including Wnt pathway wiring and downstream targets, tumour makeup, ITH, cancer type, microenvironment, and many more. The role of DKK1 in GBM isn't well documented, but it has paradoxically been shown to be hypermethylated in one study (Gotze S, 2010), and its expression in cerebrospinal fluids was shown to correlate with pathological classification and malignancy (Zhou Y, 2010). In a recent study, the ASCL1 transcription factor was shown to activate Wnt signaling through the inhibition of DKK1. Knockdown of ASCL1 lead to decreased self-renewal capacities in vitro and prolonged survival in tumour-bearing mice (Rheinbay E, 2013).

In addition to its direct role in cancer, DKK1 has been linked to CSCs, and has been shown to prevent the differentiation of osteosarcoma cells (Krause U R. D., 2014; Goldstein SD, 2016) and β-catenin signaling has been shown to correlate with glioma differentiation (Wang Y, 2013). Latency competent cancer (LCC) CSCs have been shown to be able to avoid immune clearance and impeding DKK1 expression lead to their immune clearance via the upregulation of natural killer (NK) cell activating ligands (Malladi S, 2016). Furthermore, DKK1 has been shown to have immunosuppressive abilities through signaling to myeloid-derived suppressor cells (MDSCs) (D'Amico L, 2016), by inhibiting macrophage and neutrophil recruitment in lung metastases (Zhuang X, 2017), and in a non-cancer model it was shown to antagonize T_h1 polarization and block the secretion of pro-

inflammatory IFN-G (Fridman WH, 2012). These studies raise important questions such as: does DKK1 contribute to an undifferentiated phenotype? Does it promote CSCs? Can targeting DKK1 lead to the immune clearance of CSCs such as BTICs?

DKK1 levels have been correlated with poor survival in lung, head & neck, pancreatic, oesophageal and cholangiocarcinoma cancers (The Human Protein Atlas; Yamabuki T, 2007; Shi RY, 2013). In a number of preclinical cancer models, DKK1 knockdown decreased migration, invasion, proliferation, tumour growth, metastasis, angiogenesis, and anti-DKK1 antibodies have shown efficacy in models of lung, melanoma, multiple myeloma, osteosarcoma, and prostate cancer (Kagey MH, 2017). Novartis (BHQ880) and Leap Therapeutics (DKN-01) have both developed anti-DKK1 antibodies, which are currently being investigated in clinical trials for multiple myeloma, cholangiocarcinoma, endometrial, uterine, ovarian, gallbladder, bile duct, and esophageal cancers.

This thesis describes a research project aimed at identifying novel potential therapeutic targets of GBM BTICs, which are thought to be responsible for GBM relapse, by performing differential gene expression analyses on sets of transcriptomic screens. The first profiles the evolution of patient-derived GBM samples throughout GBM disease progression – from primary tumour to relapse – using a patient-derived xenograft (PDX) model of recurrent GBM. The second screen compares the transcriptomic profiles of patient-derived BTICs with their healthy counterparts, neural stem cells. The top candidate

identified, Dickkopf-1 (DKK1), was then functionally validated before a novel antibody

modality targeting it was developed and tested *in vitro*.

MATERIALS AND METHODS

Patient-derived glioblastoma sample processing

Glioblastoma patient-derived lines (PDLs) are obtained through an ongoing collaboration with the Hamilton General Hospital where tumour samples of consenting patients are obtained following surgical removal (see Appendix for patient demographics). The tumour is first sliced into very small pieces, before being treated with 0.2 Wünsch unit/mL Liberase™ TM (Roche) to create a single-cell suspension by freeing the cells from the extracellular scaffold. The cells are filtered through a 70μm filter and incubated with a red blood cell (RBC) lysis buffer (STEMCELL) at room temperature for 5 minutes to remove the RBCs. The cells are washed with PBS and the GBM PDLs are grown as described (*see Tissue Culture*). Following confirmation from the pathologists that the tumor received is a GBM, the PDLs are further characterized for experimental use.

Tissue Culture

The GBM PDLs are grown at 37°C and 5% CO_2 in suspension or adherently using serum-free human neural stem cell NeuroCult™ media (STEMCELL), a proprietary media formulated for the selection and growth of neural stem cells supplemented with 2μg/mL heparin (STEMCELL), 20ng/mL EGF (STEMCELL), and 10ng/mL FGF (STEMCELL). Cells grown in suspension typically grow as neurospheres; cell cluster spheroids each theoretically originating form a single CSC. This method of growth is used to select for

CSCs. PDLs can also be grown adherently on laminin-coated plates. This method allows for more rapid expansion of the PDLs (with a few exceptions). Laminin-coated plates are first coated with poly-L ornithine (Sigma-Aldrich) before being coated with laminin (BD Biosciences). Cells grown adherently are dissociated using TrypLE (Thermo Fisher), whereas neurospheres are dissociated using Liberase™ TM (Roche).

Fluorescence activated cell sorting (FACS)

Neurospheres were dissociated into single cells that were resuspended in PBS supplemented with 2mM of EDTA. Cell suspensions were stained with a PE-conjugated anti-CD133 or TRA-1-85 along with matched isotype controls (Miltenyi) and incubated for 30 min on ice. Samples were run on a MoFlo XDP Cell Sorter (Beckman Coulter). Dead cells were excluded using the viability dye 7AAD. (1:10; Beckman Coulter). Compensation was performed using mouse IgG CompBeads (BD). Expression of CD133 or TRA 1-85 was defined as positive or negative based on the analysis regions set on the isotype control. Cells were sorted into tubes containing 1mL NeuroCult™ media and small aliquots of each sort tube were re-analysed to determine the purity of the sorted populations. Cells were allowed to equilibrate at 37°C for a few hours prior to use in experiments.

Transformation and plasmid preparation

Lentiviral plasmid stocks of control shGFP and shDKK1_3-5 were kind gifts from the Moffat lab (University of Toronto). Transformations were performed using a standard protocol as follows; 50µl of thawed competent E. coli Stbl3 and 10ng of plasmid DNA were added to pre-chilled tubes and pipetted gently. The suspensions were kept on ice for 30min after which the mixture was exposed to 42°C for 20 seconds. Following the heat-shock, the tubes were kept on ice for another 5min. Following incubation, 1mL SOC media was added to the tubes and incubated for 60min at 37°C. The transformed cells were then streaked on ampicillin-containing LB agar plates (100ug/mL) and allowed to grow overnight at 37°C. A single colony is selected and inoculated into 5mL of LB broth supplemented with ampicillin and allowed to grow for 8 hours before being transferred to 100mL of the broth. After a 16-hour incubation at 37°C, the bacteria are collected by centrifugation and the plasmid DNA are extracted using the GeneJET Plasmid Midiprep Kit (Thermo Fisher), according to the manufacturer's protocol. Its DNA concentration was then determined by a nanodrop spectrophotometer.

Lentiviral Production and Transduction.

Replication-incompetent lentiviruses were produced by co-transfection of the packaging vectors pMD2G and psPAX2 along with the expression vector (iRFP670, Firefly Luciferase, shGFP (5'-ACAACAGCCACAACGTCTATA-3'), shDKK1_3 (5'-

CCTGTCCTGAAAGAAGGTCAA-3'),   or   shDKK1_5   (5'-CCAGAAGAACCACCTTGTCTT-3')) in HEK 293T cells using Lipofectamine 3000 transfection reagent (Thermo Fisher) according to manufacturer's recommendations. HEK 293T cells are cultured in DMEM media (Gibco) supplemented with 10% FBS (Gibco) and grown to 1.0×10^7 cells per T-75 flasks. Viral supernatants were harvested 48 hours after transfection, filtered through a 0.45µm cellulose acetate filter and concentrated by ultracentrifugation (15,000 RPM for 2h at 4C), aliquoted and stored at -80°C for later use. Transductions were conducted by incubating the cells of interest with the lentiviruses of interest for 48 hours. The cells were then selected for those that had successfully been infected by using 0.5µg/mL (BT428, BT458, BT993) or 2.0µg/mL (BT241) of puromycin for three days.

Self-Renewal Assays

The cells of interest are dissociated into a single-cell suspension as previously detailed. A self-renewal assay is performed by sorting 250 cells per well in NeuroCult media, per population, into a 96-well plate with cell-repellent surface (Greiner Bio-One). The plate is incubated until the neurospheres are reliably observable, typically within 4-7 days, and then counted and used to estimate the mean number of spheres per 2000 cells.

Proliferation assay

Single cells are plated into a cell-repellent 96-well plate at a density of 1,000 cells/200 µL per well and incubated for five days. 20 µL of Presto Blue (Invitrogen), a fluorescent cell metabolism indicator, was added to each well 2-6h prior to the readout time point. Fluorescence was measured using a FLUOstar Omega Fluorescence 556 Microplate reader (BMG LABTECH) at excitation and emission wavelengths of 535nm and 595nm respectively. Readings were analyzed using Omega analysis software.

RT-qPCR

Cells are pelleted and frozen until they are ready to use. RNA is extracted using the Total RNA Purification Kit (Norgen Biotek) and quantified using a nanodrop spectrophotometer. Complementary DNA was synthesized from 1ug of RNA by using iScript™ Reverse Transcription Supermix (Bio-Rad) and a C1000 Thermo Cycler (Bio-Rad) with the following cycle parameters: 4 minutes at 25°C, 30 minutes at 42°C, 5 minutes at 85°C, hold at 4°C. RT-qPCR was performed using SsoAdvanced Universal SYBR®Green Supermix (Bio-Rad) and CFX Real Time System (Bio-Rad) with the following cycles: an initial 1 cycle denaturation step for 3 min at 95°C, 39 cycles of PCR (95°C for 20s, 60°C for 20s and 72°C for 20s), 1 cycle of melting and 1 cooling cycle. Average data collection and detection of fluorescent product was performed at the end of the 72°C extension period. Products specificity was assessed by performing melting curve

analysis and examining the quality of amplification curves. Gene expression was quantified by using CFX manager software, and expression levels were normalized to 28srRNA expression. The forward primer used for DKK1 was 5'-CTCGGTTCTCAATTCCAACG-3', and the reverse primer was 5'-GCACTCCTCGTCCTCTG-3'. The forward primer for 28S was 5'-AAGCAGGAGGTGTCAGAAA-3' and the reverse was 5'-GTAAAACTAACCTGTCTCACG-3'.

Western Blotting

Cells are pelleted and frozen until ready to use. Cell are lysed using in-house RIPA buffer supplemented with Halt™ Protease & Phosphatase Inhibitor Cocktail (Thermo Fisher) and the protein content is quantified using the DC™ Protein Assay Kit (Bio-Rad), as per manufacturer's protocol. Denatured total protein (10μg) in NuPAGE LDS Sample Buffer (Invitrogen) was separated using 10% sodium dodecyl sulphate-polyacrylamide gel electrophoresis and transferred to polyvinylidene fluoride membrane. Western blots were probed with the following primary antibodies: DKK1 (Abcam, ab109416) and β-Tubulin (Abcam, ab6046). The secondary antibody was horseradish peroxidase conjugated goat anti-rabbit IgG (Bio-Rad). The bands were visualized using Luminata™ Forte Western HRP Substrate (Millipore) and Chemidoc (Bio-Rad).

Anti-DKK1 IgG monoclonal antibody treatment

Human anti-DKK1 IgG monoclonal antibodies were provided by the Centre for the Commercialization of Antibodies and Biologics (CCAB). The cells were incubated with the designated concentration of antibodies.

Tumour Engraftment (Surgeries)

Human-mouse patient-derived xenografts (PDX) are produced by injecting 10^6 GBM PDL cells into the right frontal lobe of immunocompromised NOD scid gamma (NSG) mice. Briefly, mice were anaesthetized using 2.5% Isoflurane. The area of incision is disinfected using iodine and ethanol before an incision is made. A small burr hole is made (2-3 mm anterior to the coronal suture, 3 mm lateral to midline) using a drill held perpendicular to the skull. A Hamilton syringe is used to inject 10μl of cell suspension into the frontal lobe. The incision is closed using interrupted stitches and sutures were sealed with a tissue adhesive. Mice are placed in recovery cages and monitored weekly for signs of illness.

Chemotherapy and Radiation Treatment

Once the GBM PDLs are shown to have engrafted via MRI imaging, the mice are randomly assigned to control or treatment group. The mice are treated with chemotherapy

and radiation in order to for the treatment regimen to resemble how patients are treated as closely as possible. The PDX mice are treated with 50mg/kg of TMZ by oral gavage (equivalent to 150mg/m^2; GBM patients receive 75 to 200mg/m^2) daily for 5 days straight. On the first day, mice are irradiated one hour after the administration of TMZ to allow it to properly enter the bloodstream and exert its effect prior to the irradiation. Throughout the five days, and the two weeks following treatment, the mice lose a substantial amount of weight and are given fluids in order to keep them hydrated. Mice are monitored daily after treatment until the end of the experiment.

Recurrence and Endpoint Monitoring

Tumour-bearing mice are monitored daily for any signs of sickness including reduced movement, ruffled fur, reddened eyes, open wounds, and weight loss. Mice are also periodically imaged via MRI or IVIS to monitor tumour growth.

***In vivo* tumour imaging**

GBM *in vivo* engraftment and progression is tracked by *in vivo* imaging using MRI, and either fluorescence (iRFP670) or bioluminescence (firefly-luciferase). MRI is conducted by collaborators in the Bock laboratory at McMaster University, whereas *in vivo* imaging is conducted using an IVIS Spectrum (PerkinElmer). Animals are rendered unconscious using isoflurane and the engrafted GBMs are imaged.

H&E Staining

Mice are anesthetised and rendered unconscious using Avertin (tribromoethanol) before being perfused using 10% formalin. The brain is then extracted and left in 10% formalin for 48 hours before being sliced and sent for paraffin-embedding and H&E staining.

RNA-sequencing

Samples of the recurrent GBM PDX *in vivo* pipeline (Project 1) were sequenced using paired-end RNA-Seq at a depth of 50M reads per sample by MedGenome Inc. Bioinformatics analysis was conducted by Dr. Kevin Brown of the Moffat laboratory (University of Toronto). Reads were mapped to the human genome (GRCh37/hg19) using the STAR aligner software before being normalized for depth.

Samples of the GBM BTIC *in vitro* analysis (Project 2) were sequenced using paired-end sequencing at a depth of 125M reads per sample by the University of Toronto's Donnelly Sequencing Centre. Bioinformatics analysis was conducted by Dr. Jeff Liu of the Bader laboratory (University of Toronto). Reads were mapped to the human genome (GRCh38) using the STAR aligner software before being normalized for counts-per-million using the edgeR software and subjected to CPM-cutoff of 3.5 reads.

RESULTS

Project 1: Establishment of a PDX pipeline for the identification of novel therapeutic targets in recurrent glioblastoma

In order to identify targets of rGBM, an *in vivo* patient-derived GBM pipeline was established in order to study what we deemed to be three key time-points of GBM disease progression – the primary tumour, post-therapy remission, and the recurrence – along with an additional two key experimental control time-points in order to help quantify the effects of *in vitro* culturing both on the initial tumour and prior to *in vivo* use. Altogether, the five time-points include the initial patient tumour sample, a pre-engraftment *in vitro* sample (the GBM PDL cells grown in culture before being engrafted), tumour engraftment, the post-treatment stage of minimal residual disease (MRD), and tumour recurrence (Figure 1a).

The first time-point, the initial patient tumour sample, is collected as soon as possible a few hours post-surgical resection. The tumour sample is taken from the hospital operation room to the laboratory where it is cut into fine pieces before it is either processed or snap-frozen. The latter is what serves as the patient tumour sample in our pipeline (Figure 1a). The rest of the patient tumour is processed into a stable PDL as described (see Materials and Methods). Unfortunately, finding good GBM patient-derived lines (PDLs) is difficult, as these must be able to (1) survive processing and grow at a reasonable pace *in vitro*, (2) engraft and form tumours *in vivo*, (3) respond to chemotherapy and radiotherapy and enter tumour remission (reduction of tumour burden), and (4) cause a
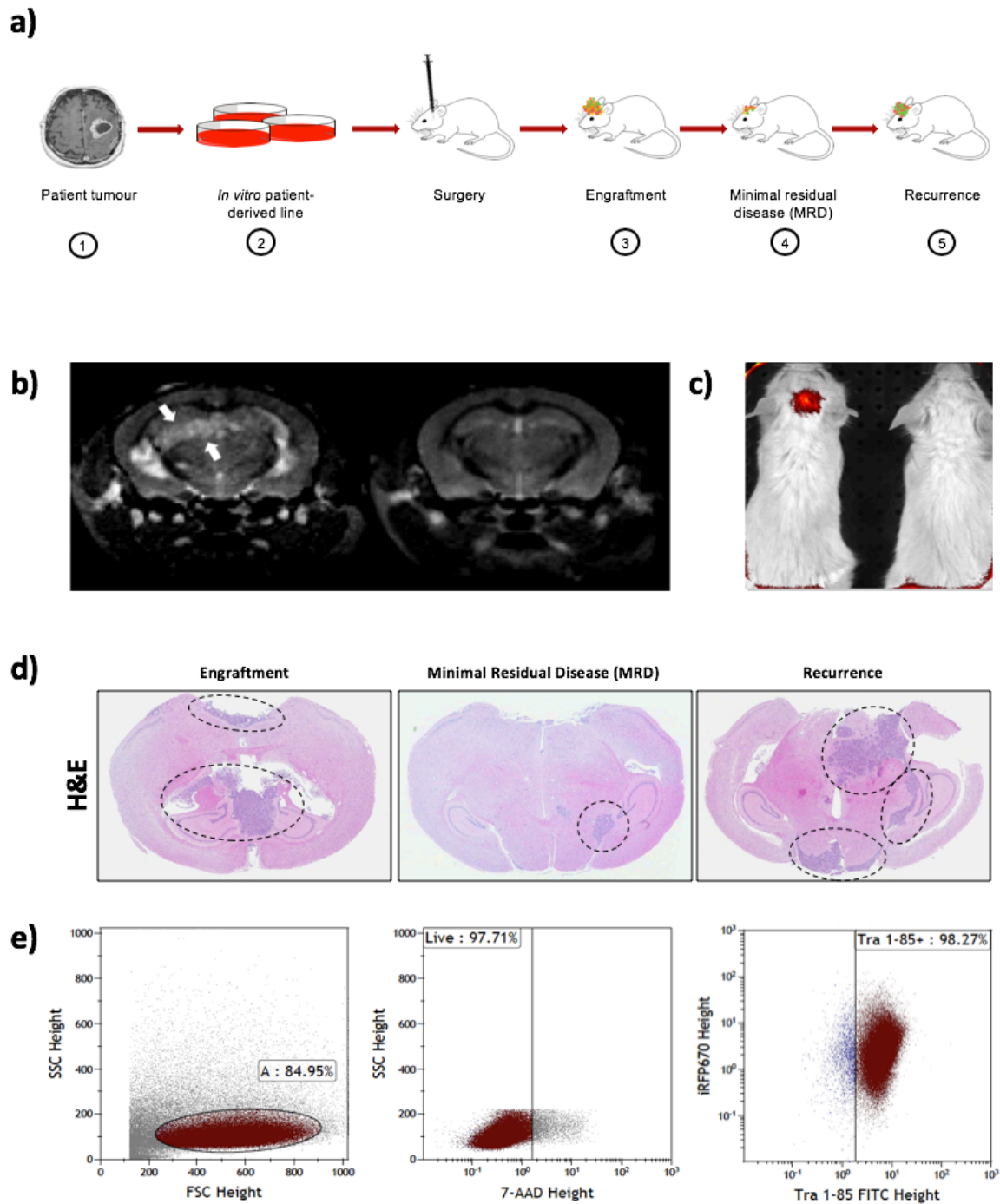
Figure 1. Patient-derived xenograft model-based sample acquisition pipeline for recurrent glioblastoma. (**a**) Schematic of the five samples collected including (1) the patient tumour sample, (2) *in vitro* culture prior to injection, (3) engraftment, (4) the post-

treatment stage of minimal residual disease (MRD), and (5) tumour recurrence. (**b**).

Representative MRI scan of a tumour-bearing PDX mouse (left) and a health control mouse

(right). The tumour is demarcated by the white arrows. (**c**) Representative IVIS imaging

of tumour-bearing mice. The left mouse bears a tumour expressing an iRFP670 reporter,

and the right mouse's tumour does not. (**d**) Representative H&E stained brain tissue slides

of the engraftment, MRD, and recurrence stages of tumour progression using a PDX model,

demonstrating the effectiveness of the treatment regimen in reducing tumour burden and

causing tumour relapse. (**e**) Representative isolation of tumour cells by FACS sorting using

the TRA 1-85 human-specific antibody. The left panel shows the selection of cells among

the background; the middle panel demonstrates the selection of live cells; and the right

panel demonstrates the isolation of live human TRA 1-85 positive cells from the remaining

mouse cells.

relapse of the initial GBM tumour. Less than a quarter of patient-derived lines seem to fit that description based on preliminary work conducted in the laboratory. Why that is the case remains unclear at this point but it indicates that numerous selection pressures are at play, suggesting our methods may only allow us to study a fraction of the total GBM population (discussed later).

PDLs that survive tumour processing and grow *in vitro* are then tested for engraftment using 5×10^5 or 10^6 cells. These are injected into NOD SCID gamma (NSG) mice, and the tumour progression is monitored using magnetic resonance imaging (MRI) until a tumour mass is spotted (Figure 1b), which typically takes anywhere from 4-12 weeks. After engraftment is shown by MRI, the results are validated by hematoxylin and eosin (H&E) staining (Figure 1d). Only the PDLs which do form tumours were used in this study. Once a PDL is shown to be able to engraft, they are transduced with either iRFP670 (Shcherbakova DM, 2013) or firefly luciferase in order to monitor tumour progression *in vivo*. We were only able to scan the mice using MRI once per week, so adding a fluorescent (iRFP670) or bioluminescent (firefly-luciferase) probe was done to track progression on a more constant basis. The lines were initially transduced with iRFP670 because of its stated sensitivity and use *in vivo* (Figure 1c), however the images that were obtained were not consistent and we have not yet been able to optimize its use. It was then decided to switch to a more commonly used probe, firefly luciferase, in order to track tumour progression. Other uses for the markers included being able to select for cells properly transduced thanks to either a puromycin-resistant (firefly luciferase) or

hygromycin-B-resistant (iRFP670) genes that were included in the transduced plasmid, and to be able to isolate the GBM PDLs from the mouse brain cells while collecting samples for RNA-sequencing. We later decided to simply use TRA 1-85, a human cell-specific antibody, to isolate the GBM cells from the mouse cells by FACS (Figure 1e). The PDLs expressing one of the two probes (the data presented in this thesis only includes PDLs expressing iRFP670) are then once again injected into mice, and the mice divided into the following cohorts: engraftment control, MRD, MRD control, recurrence, and recurrence control. In some cases, the MRD and recurrence controls end up being the same cohort as the mice succumb to their tumour burden faster with some PDLs compared to others. Once engraftment is confirmed, the engraftment control cohort is sacrificed and we are able to obtain our third time-point: tumour engraftment.

In order to establish this data-acquisition pipeline, we used a human-mouse PDX model of the disease previously developed by other members of the research group where PDL cells are injected intracranially into the right frontal lobe of the mice as described (Materials and Methods). To replicate patient-treatment and obtain clinically relevant samples, we devised a treatment regimen that most closely resembled what patients receive in clinics and hospitals (Stupp R, 2005). Once tumours are successfully engrafted, the tumour-bearing mice are treated with clinically relevant doses of chemotherapy (temozolomide; TMZ) and radiation. TMZ is given for 5 straight days at 50mg/kg orally, and 2Gy of whole-brain radiation is given only on the first day of treatment. In the clinic, patients are treated orally with 75-200mg/m^2 of TMZ daily for 5 straight days and are treated with 2Gy of focal radiation daily for 30 days. 50mg/kg of TMZ dosage in mice is

equivalent to 150mg/m^2 in humans according to FDA guidelines (Reagan-Shaw S, 2008). Unfortunately, 2Gy of radiation on the first day of treatment was the most clinically relevant dose we could achieve without unduly harming the mice. The control mice are treated with standard saline solution and are not subjected to radiation treatment. Our fourth time-point, MRD, which represents the point at which the tumour burden is at its lowest, is collected two weeks post-treatment. From this point on, the mice are monitored using MRI, an In Vivo Imaging System (IVIS) to detect either fluorescence or bioluminescence, and using physical cues (body weight, ruffled fur, reduced movement, etc.) until the tumour relapses and the mice reach endpoint. Once they do, we are able to obtain our final time-point: tumour recurrence.

Cells from each of the five time-points are then snap-frozen and sent out for RNA sequencing (MedGenome Inc.). Samples obtained from the PDXs are isolated and purified from the mouse cells thanks to the following. The culturing media, NeuroCult™ media, itself is optimized for human neural stem cell (NSC) growth, and thus should select for human cells. As the GBM PDLs have also been rendered either puromycin (firefly-luciferase) or hygromycin-B-resistant (iRFP670), the cultures are then grown in the presence of the appropriate antibiotic to select for these cells. Finally, the GBM PDLs are isolated from the remaining mouse cells by FACS using the human-specific TRA 1-85 antibody (Figure 1e). Once the cells have been purified, they are grown, snap frozen, and sent off for RNA sequencing.

A number of primary GBM PDLs have been shown to engraft but failed to recur. Until now, only the following have been shown to be successful or to still hold potential to be used for the proposed model: BT428, BT459, BT799, BT935, BT993, MBT06. Of those lines only BT428 and BT935 successfully recurred. BT799 failed to recur but was otherwise successful, BT459 and BT993 failed to engraft despite being previously shown to be capable, and experiments using additional PDLs are ongoing (Figure 2).

BT428 cells were injected using $1.0x10^6$ cells and were able to engraft 46 days post-surgery (Figure 2a). MRD samples were collected two weeks after the mice were treated with TMZ and radiation, and the recurrence samples were collected when the tumours recurred approximately 6.5 months later. The control mice treated with saline solution reached endpoint two weeks after MRD, in comparison. Tumours from BT428 are very diffuse and the most difficult to see by MRI compared to BT799 and BT935. For example, tumours are very difficult to detect by MRI in the MRD and MRD control samples. Even in the engraftment and recurrence MRI scans, irregularities and disturbances can be noticed in the engraftment MRI scan, it is not easy to pinpoint where exactly the tumour is situated. This panel demonstrates why it is important to not rely solely on MRI to track tumour development. The accompanying H&E staining images confirmed tumour presence in all cases with the exception of the MRD samples, which is to be expected since this stage represents the point in time where the tumour burden is at its lowest. The recurrence control mouse cohort perished approximately one week after MRD and no additional MRI scan was performed on time. The MRD control scan thus represents the last scan conducted on this cohort.
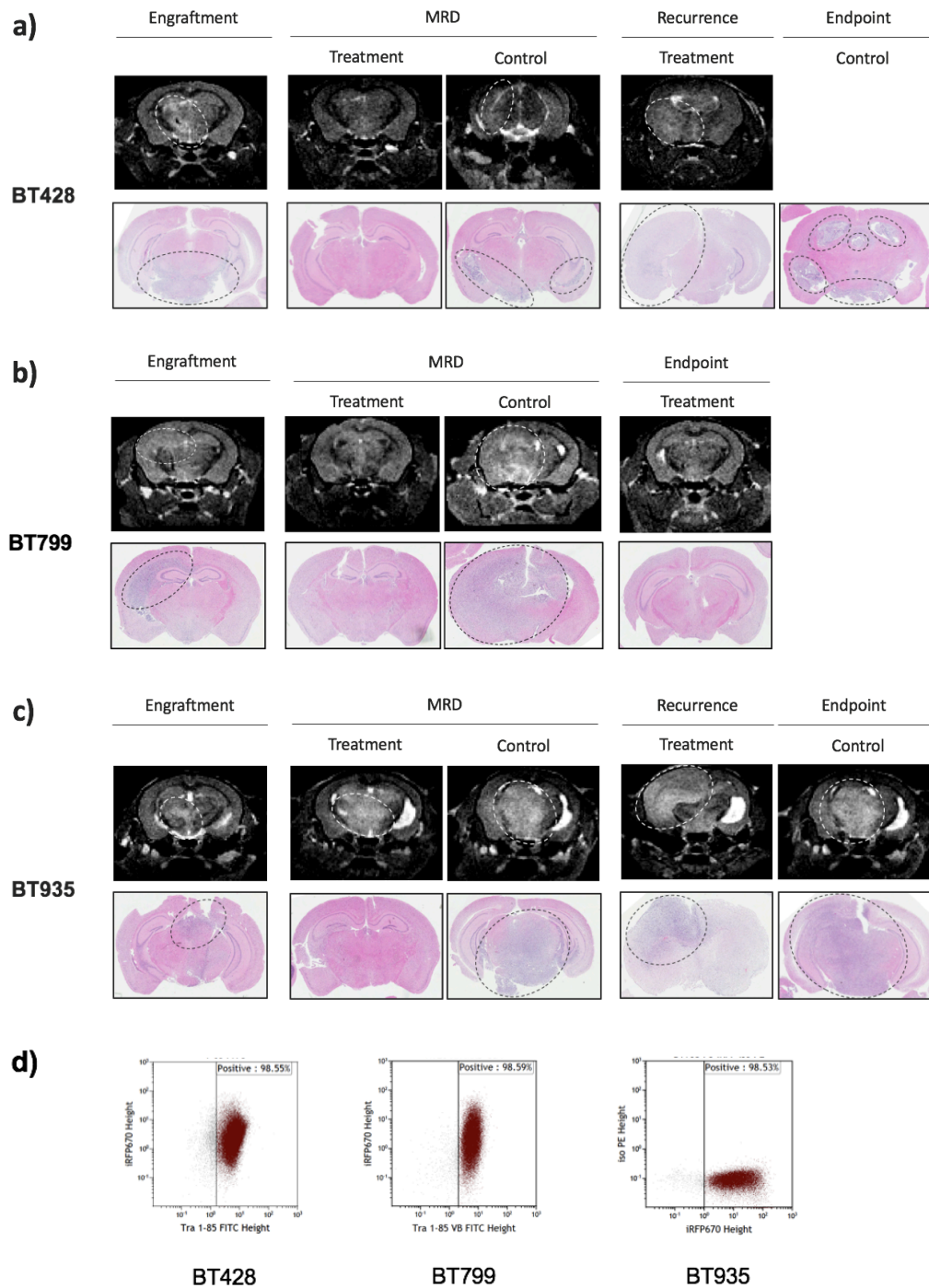
Figure 2. Patient-derived xenograft recurrent GBM tumour progression and tumour cell isolation. (**a-c**) BT428, BT799, and BT935 GBM PDLs were injected as described. Representative MRI scans and H&E stained tissue slides of the respective tumour

engraftment, MRD (remission), and recurrence depict each tumours progression. Engraftment represents the engraftment of the primary tumour after the injections. MRD illustrates a reduction in tumour burden two weeks post-treatment with 2Gy of radiation and daily 50mg/kg of TMZ for 5 days. MRD Ctrl demonstrates the tumour burden of mice that did not receive TMZ or radiation. Recurrence represents the relapsed tumour post-treatment. Recurrence Ctrl represent the endpoint of mice not treated with chemotherapy or radiation. (**d**) Samples collected at each time-point shown in a-c were isolated by FACS either using the human cell-specific TRA 1-85, or iRFP670 reporter. BT935 engraftment, MRD and MRD Ctrl were the only samples isolated using the iRFP670 reporter.

BT799 cells were able to engraft 27 days after being injected using 1.0×10^6 cells as well (Figure 2b). Both the MRD and MRD control samples were collected two weeks after treatment. The difference between the mice treated with chemotherapy and radiation (MRD) compared to the control mice given saline (MRD control) is staggering as virtually no cancerous tissue is seen in the treated mice in comparison to the enormous tumour mass seen in the control (Figure 2b). The recurrence (or endpoint) controls all perished three to six days later, thus we were not able to image the mice by MRI during that time. Unfortunately, the tumours did not recur until the mice reached endpoint, 12 months post-treatment. Why the tumours did not recur is not known as previous experiments using the same chemoradiotherapy regimen with the BT799 PDLs yielded recurrent tumours. Although the difference between the MRD and its control clearly demonstrates the efficacy of our chemoradiotherapy regimen, especially in comparison to the results obtained in Figure 2a, the lack of recurrence in this case could point to the need for further optimization.

BT935 was the only PDL injected using 5.0×10^5 cells, and tumours engrafted 57 days after the fact (Figure 2c). Once again MRD samples were collected two weeks post-treatment, and the treated mice had their tumours relapse approximately 4 months later. The control mice reached endpoint two weeks after MRD. In contrast with BT428 and BT799, cancerous tissue can be seen by MRI in the MRD samples indicating that BT935 is more resistant to TMZ and radiation compared to the other two PDLs. Interestingly, H&E slides of the MRD samples show little-to-no GBM presence. It is important to note that the MRI scans and H&E slides are representations of each time-point and they are not necessarily taken from the same animal, which they were not in this case.

Prior to sending the samples for RNA-sequencing, the engraftment, MRD, and MRD control cells were purified and isolated as described (see *Methods and Materials*) from the few remaining mouse cells by FACS before being sent out for RNA-sequencing (Figure 2d). BT935 was isolated based on an iRFP670 fluorescence expression instead of TRA 1-85 expression like BT428 and BT799. This is because it was the first line used in this pipeline and we have since decided to isolate based on TRA 1-85, which selects specifically for human cells and should thus improve the accuracy of our results. The frozen samples were then sent out to MedGenome for paired-end RNA sequencing at a depth of 50M reads. Analysis of the data was conducted by Dr. Kevin Brown of the Moffat laboratory where the depth-normalized read counts were calculated to identify the transcripts that had been the most upregulated in the MRD samples of each PDL in comparison to both their engraftment and MRD control samples. Experiments aiming to validate the top hits from this RNA-Seq screen is ongoing and being conducted by other members of the Singh and Moffat laboratories.

Project 2: Identification of DKK1 as a novel GBM target by differential gene expression

In order to identify novel target markers of GBM BTICs, a second RNA-Seq screen was conducted *in vitro* on patient-derived GBM BTICs (GBM tumour initiating cells; GBM cancer stem cells) and patient-derived healthy foetal neural stem and progenitor cells (NSPCs). In this study, four arbitrarily chosen GBM (BT428, BT458, BT624, BT698) and NSPC (NSC194, NSC195, NSC198, NSC200) PDLs were sorted by FACS into four populations based on the CD133 marker: CD133+ GBM, CD133- GBM, CD133+ NSPC, CD133- NSPC. The purpose of the study was to compare the transcriptomic profiles of each population in order to ideally identify novel GBM BTIC markers, which in this case are considered to be the GBM CD133+ population. Pellets from each were snap frozen and sent for RNA sequencing at the University of Toronto's Donnelly Sequencing Centre. The sequencing results were subsequently analyzed by Jeff Liu of the Bader laboratory (University of Toronto) where the gene expression profiles of all populations were compared in the following manner: (1) CD133+ vs CD133- GBMs, (2) CD133+ vs CD133- NSPCs, (3) CD133+ GBMs vs NSPCs, and (4) CD133- GBMs vs NSPCs (Figure 3). Unfortunately, the following samples did not pass quality control and could not be used in the analysis: BT428 CD133+, BT624 CD133+, and NSPC198 CD133-. This means while four biological replicates were used to generate the CD133- GBM and CD133+ NSPC data, only two biological samples were used to generate the CD133+ GBM data, and three for the NSPC CD133- data.

Lists of the most differentially expressed genes were generated by the Bader laboratory for each of the four comparisons (Table 1-4). Prominin-1 (PROM1), also known as CD133, was the fourth highest hit in the CD133+ vs CD133- GBM comparison, serving as a validation of the screen. The generated lists were then shortened based on numerous factors such as human tissue expression (low expression in healthy tissue, especially brain, is preferred), cell localization (i.e. cell membrane, extracellular matrix, secreted proteins), expression in healthy tissue in comparison with tumour tissue (i.e. healthy brain vs. GBM), expression in recurrent GBM compared to primary GBM, marker expression effects on survival, known marker physiological function, previous association with cancer, and the heightened expression in the CD133+ and BTIC populations of the four comparisons. The information used to shorten these lists were obtained from public databases such as The Cancer Genome Atlas (TCGA), The Human Protein Atlas, GeneCard, and UniProt. This yielded a list of 12 top targets (Table 5), with the top target being Dickkopf-1 (DKK1).
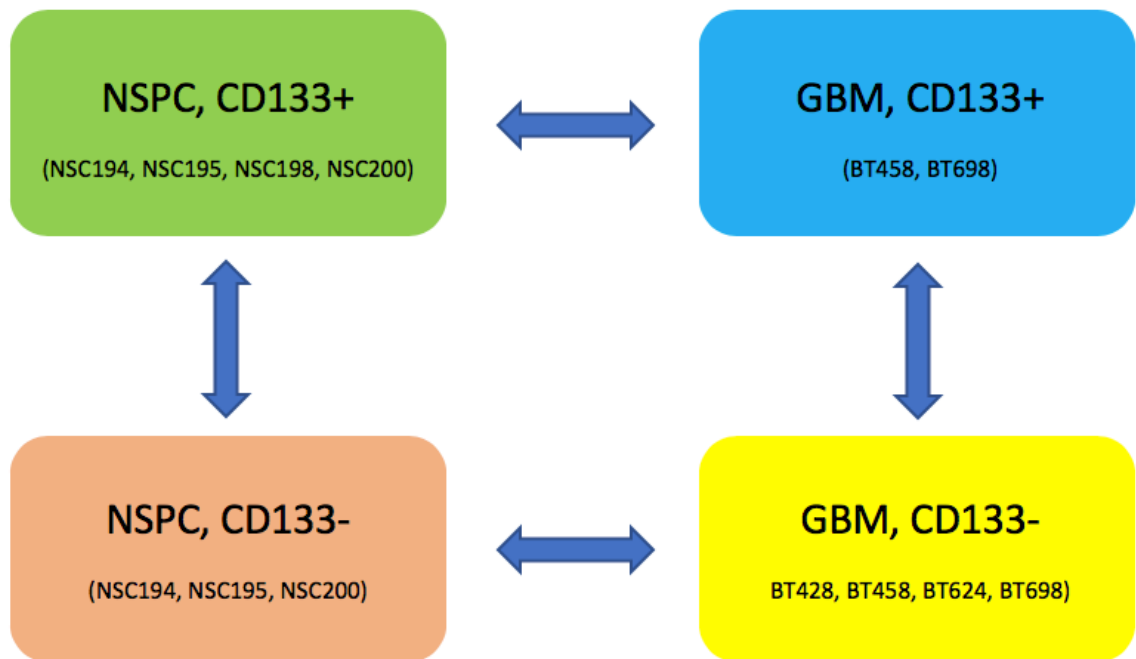
Figure 3. Four gene expression differential comparisons conducted in Project 2. Differential gene expression analyses were conducted between the four groups illustrated in order to identify novel candidate targets of GBM BTICs. Populations of the PDLs listed were sorted by FACS according to CD133 (prominin-1), a well established marker of BTICs and NSCs. The CD133+ populations BT428 and BT624, and the CD133- population of NSC198 did not pass quality control during RNA-sequencing. The RNA-Seq data generated was analyzed and aligned to the human genome (GRCh38) using the STAR aligner software by Dr. Jeff Liu.

Table 1. Top hits of differentially expressed genes in CD133+ compared to CD133-glioblastoma populations. Cell pellets of BT428, BT458, BT624, and BT698 were sorted by FACS based on CD133. CD133+ population sample of BT428 and BT624 did not pass quality control and were not included in the analysis. Samples were sent for RNA-sequencing at the Donnelly Sequencing Centre, and reads were aligned to the human genome (GRCh38) using the STAR aligner and the analysis was performed by Dr. Jeff Liu.

Gene	Log$_2$FC	p-value
MYCN	2.48	0.08
WNT7B	2.36	0.11
ANKRD33B	1.88	0.06
PROM1	1.56	0.08
CDCA5	1.55	0.09
CDC42EP2	1.50	0.12
FOSL1	1.42	0.09
EPAS1	1.34	0.13
HAS3	1.24	0.11
NFKB1	1.22	0.10
NELL1	-4.00	0.14
RORB	-4.44	0.08
FRAS1	-4.53	0.09
MIR4458HG	-4.58	0.05
SDK2	-4.62	0.08
FAM69C	-4.72	0.09
ARHGAP36	-5.15	0.11
GPD1	-6.29	0.09
DLX6-AS1	-6.90	0.13
ST8SIA3	-7.21	0.05

Table 2. Top hits of differentially expressed genes in CD133+ compared to CD133-neural stem and progenitor cell populations. Cell pellets of NSC194, NSC195, NSC198, and NSC200 were sorted by FACS based on CD133. CD133- population sample of NSC198 did not pass quality control and was not included in the analysis. Samples were sent for RNA-sequencing at the Donnelly Sequencing Centre, and reads were aligned to the human genome (GRCh38) using the STAR aligner and the analysis was performed by Dr. Jeff Liu.

Gene	Log_2FC	p-value
AGT	4.42	0.04
FGFBP2	4.02	0.00
COL18A1	3.35	0.00
ARSI	3.02	0.00
SLC6A20	2.98	0.01
GPX3	2.87	0.01
COL8A1	2.82	0.01
IFITM1	2.77	0.01
C1QTNF1	2.76	0.00
OLFML2A	2.75	0.00
PHACTR3	-5.61	0.00
TNR	-5.61	0.00
EPHA5	-5.79	0.00
MYOT	-5.85	0.00
PTPRR	-5.96	0.00
NRXN1	-5.99	0.00
HMP19	-6.63	0.00
SPHKAP	-6.82	0.00
VSTM2A	-7.01	0.00
MYT1L	-7.08	0.00

Table 3. Top hits of differentially expressed genes in CD133+ populations of glioblastoma compared to CD133+ populations of neural stem and progenitor cells. Cell pellets of BT428, BT458, BT624, BT698 and NSC194, NSC195, NSC198, and NSC200 were sorted by FACS based on CD133. CD133+ population sample of BT428 and BT624 did not pass quality control and were not included in the analysis. Samples were sent for RNA-sequencing at the Donnelly Sequencing Centre, and reads were aligned to the human genome (GRCh38) using the STAR aligner and the analysis was performed by Dr. Jeff Liu.

Gene	Log_2FC	p-value
WBSCR17	10.24	0.00
MTAP	9.74	0.00
CBLN4	9.66	0.00
ST8SIA3	9.59	0.00
KLHL9	9.36	0.00
RANBP17	9.19	0.00
MYO3A	9.15	0.00
ZIC3	8.95	0.00
SNCA	8.91	0.00
CDKN2B	8.68	0.00
HAGLR	-8.56	0.00
KRT16	-8.74	0.00
POSTN	-8.76	0.00
SAMD5	-8.86	0.00
EYA1	-8.95	0.00
LINC01116	-8.97	0.00
CYP1B1	-9.12	0.00
COL19A1	-9.14	0.00
EBF1	-9.18	0.00
SHOX2	-10.04	0.00

Table 4. Top hits of differentially expressed genes in CD133- populations of glioblastoma compared to CD133- populations of neural stem and progenitor cells. Cell pellets of BT428, BT458, BT624, BT698 and NSC194, NSC195, NSC198, and NSC200 were sorted by FACS based on CD133. The CD133- population of NSC198 did not pass quality control and was not included in the analysis. Samples were sent for RNA-sequencing at the Donnelly Sequencing Centre, and reads were aligned to the human genome (GRCh38) using the STAR aligner and the analysis was performed by Dr. Jeff Liu.

Gene	Log_2FC	p-value
ZIC3	10.09	0.00
CALB2	9.75	0.00
GAD2	8.99	0.00
SYNPR	8.68	0.00
LRRC3	8.56	0.00
NNAT	8.40	0.00
OTX2	8.07	0.00
DPP10	7.94	0.00
CLVS2	7.90	0.00
RANBP17	7.81	0.00
DKK1	-8.57	0.00
KCNE4	-8.63	0.00
PITX1	-8.72	0.00
HOXA3	-8.94	0.00
EN1	-9.01	0.00
HOXD10	-9.31	0.00
POSTN	-9.52	0.00
MEOX2	-9.53	0.00
CFH	-9.70	0.00
SHOX2	-9.71	0.00

Table 5. Refined list of top-12 candidate targets of glioblastoma. Hits generated from the differential genes expression analyses (top hits in tables 1-4) were refined based on the listed factors. Data from the last two columns was obtained via the RNA-Seq analysis of patient-derived GBMs and NPSCs. Information located in the other columns originate from these publicly available databases: The Cancer Genome Atlas, The Human Protein Atlas, GeneCard, and UniProt. The genes were selected based on cellular localization, expression in primary and recurrent GBM, human tissue expression (not shown), survival advantages, and the determined flow changes (FC) calculated during RNA-Seq analysis.

Gene	Localization	Primary GBM	Recurrent GBM	Survival	Population comparisons	$\log_2$FC	FC
DKK1	Secreted	Higher	Not enough data points	No significance	NPSC vs GBM (CD133+)	-8.57	380.038034
					NPSC vs GBM (CD133-)	-7.34	162.016844
					CD133+ vs CD133- (GBM)	-0.08	1.05701804
					CD133+ vs CD133- (NPSC)	N/A	N/A
CFH	Membrane Extracellular Vesicles	Higher (Debatable, not many data points)	N/A	No significance	NPSC vs GBM (CD133+)	-9.7	831.746454
					NPSC vs GBM (CD133-)	N/A	N/A
					CD133+ vs CD133- (GBM)	-0.43	1.34723358
					CD133+ vs CD133- (NPSC)	N/A	N/A
KCNE4	Membrane	Higher	Not enough data points	Low expression advantage	NPSC vs GBM (CD133+)	-8.63	396.176638
					NPSC vs GBM (CD133-)	-6.76	108.3834
					CD133+ vs CD133- (GBM)	0.27	1.20580783
					CD133+ vs CD133- (NPSC)	N/A	N/A
GPNMB	Membrane	Higher	Not enough data points	Low expression advantage	NPSC vs GBM (CD133+)	-5.53	46.2057343
					NPSC vs GBM (CD133-)	-5.18	36.2522843
					CD133+ vs CD133- (GBM)	-1.62	3.07375036
					CD133+ vs CD133- (NPSC)	N/A	N/A
OLFML3	Extracellular matrix	Higher	Lower	No significance	NPSC vs GBM (CD133+)	-5.94	61.3929036
					NPSC vs GBM (CD133-)	N/A	N/A
					CD133+ vs CD133- (GBM)	-0.92	1.89211529
					CD133+ vs CD133- (NPSC)	N/A	N/A
TSPAN9	Membrane	Higher (Debatable, not many data points)	Equal	No significance	NPSC vs GBM (CD133+)	-2.21	4.62675274
					NPSC vs GBM (CD133-)	-2.23	4.6913398
					CD133+ vs CD133- (GBM)	0.69	1.61328352
					CD133+ vs CD133- (NPSC)	0.71	1.63580412
LHFPL2	Membrane	Higher	Lower	No significance	NPSC vs GBM (CD133+)	-2.1	4.28709385
					NPSC vs GBM (CD133-)	-1.33	2.51402675
					CD133+ vs CD133- (GBM)	-0.19	1.14076372
					CD133+ vs CD133- (NPSC)	0.62	1.53687518
SAMD5	Unknown (likely membrane)	N/A	N/A	N/A	NPSC vs GBM (CD133+)	N/A	N/A
					NPSC vs GBM (CD133-)	-8.86	464.649808
					CD133+ vs CD133- (GBM)	0.84	1.79005014
					CD133+ vs CD133- (NPSC)	N/A	N/A
C5orf38	Secreted	N/A	N/A	N/A	NPSC vs GBM (CD133+)	N/A	N/A
					NPSC vs GBM (CD133-)	-8.31	317.365171
					CD133+ vs CD133- (GBM)	0.873	1.83146737
					CD133+ vs CD133- (NPSC)	N/A	N/A
LRRN4CL	Membrane Extracellular matrix	N/A	N/A	N/A	NPSC vs GBM (CD133+)	-4.55	23.4253711
					NPSC vs GBM (CD133-)	-4.75	26.9086853
					CD133+ vs CD133- (GBM)	-0.51	1.4240502
					CD133+ vs CD133- (NPSC)	N/A	N/A

AFAP1L1	Membrane	N/A	N/A	N/A	NPSC vs GBM (CD133+)	-3.26	9.57982964
					NPSC vs GBM (CD133-)	N/A	N/A
					CD133+ vs CD133- (GBM)	-0.32	1.24833055
					CD133+ vs CD133- (NPSC)	N/A	N/A
HAS3	Membrane Extracellular matrix	N/A	N/A	No significance	NPSC vs GBM (CD133+)	-0.49	1.40444488
					NPSC vs GBM (CD133-)	-0.92	1.89211529
					CD133+ vs CD133- (GBM)	1.24	2.36198532
					CD133+ vs CD133- (NPSC)	0.83	1.77768536

Project 3: Validation of DKK1 as a potential therapeutic target for glioblastoma

DKK1 was selected from the list of targets obtained in a large part because it was highly upregulated in both the CD133+ and CD133- population of the GBM samples compared to their NSPC counterparts. This however makes it simply a target of GBM and not GBM BTICs, which was the initial aim of the study. DKK1 had a $\log_2$ fold-change (FC) of 8.57 (380x upregulation) in the CD133- population of the GBMs compared to the CD133- NSPCs, and a $\log_2$FC of 7.34 (162x upregulation) in the CD133+ GBMs compared to the CD133+ NSPCs (Table 5). There was virtually no difference between the CD133+ and CD133- populations within either GBMs ($\log_2$FC = 0.08) or NSPCs (no significant difference). Additionally, DKK1 stood out as a good candidate because of its association with numerous cancers, it being upregulated in both primary and recurrent GBM in public databases such as the TCGA, and its accessibility (being a secreted protein) (Table 5).

After establishing that DKK1 was a good candidate marker for GBM in the BTIC RNA-Seq screen, its candidacy was further enforced by the fact that is was found to be upregulated in the MRD sample of BT428 in comparison to both its MRD control (by a factor of 5.72) and in its engraftment control sample (by a factor of 5.30) (Figure 4). Its expression rising in the MRD sample is significant because it indicates that DKK1 may identify a small subpopulation of cells able to survive chemotherapy and radiation *in vivo* at a higher rate than the vast majority of the other tumour cells. The RNA profile of the MRD sample of BT935 failed to be sequenced at MedGenome since the sample did not
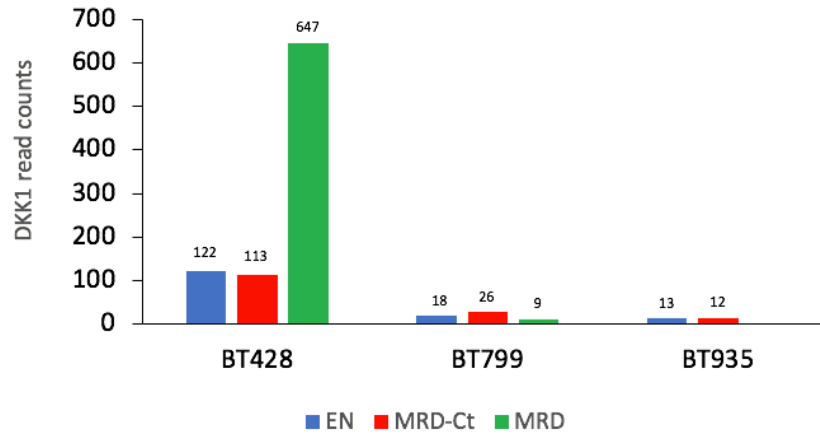
Figure 4. DKK1 expression is upregulated at the stage of MRD in BT428. DKK1 expression levels increased by a factor of 5.72 and 5.30 in the MRD sample of BT428 compared to its MRD control (MRD-Ct) and engraftment controls, respectively. DKK1 raw read counts determined by paired-end RNA-Seq analysis. Data aligned to the human genome (GRCh37/hg19) using the STAR aligner software by Dr. Kevin Brown.

pass quality control. The MRD sample of BT799 remained relatively unchanged in comparison to both its engraftment and untreated controls.

DKK1 expression maintains stemness potential of GBM patient cells

In order to validate DKK1 as a potential therapeutic target of GBM, we then decided to survey a handful of GBM PDLs and identified three that highly expressed DKK1 out of a total of ten. BT241, BT458, and BT993 expressed DKK1 at rates of 16, 84, and 85-times higher than the line with the lowest expression (BT698), respectively (Figure 5a). BT458 and BT993 are primary GBM lines whereas BT241 is a recurrent line (see Appendix for patient demographics).

The next step that was taken was to conduct functional assays of DKK1 using short-hairpin RNA (shRNA) knock-downs of DKK1. Five DKK1 shRNAs (shDKK1) were obtained from the Moffat laboratory's (University of Toronto) genome-wide shRNA library and had been validated on HAP1 cells, human near-haploid fibroblast-like cells derived from chronic myelogenous leukemia (Figure 5b). The two most efficient shRNAs, shDKK1_3 (74% knock-down) and shDKK1_5 (77% knock-down), were chosen for experimentation. The two were tested by RT-qPCR and western blotting on the three high-expression DKK1 lines (BT241, BT458, and BT993) and had the following effects (Figure 5c-e). Both shDKK1s had a much more significant effects on the transcription of DKK1 compared to its translation. In BT241, shDKK1_3 and shDKK1_5 decreased DKK1 gene

a)

b)

c) BT241

RT-qPCR   Proliferation   Self-Renewal

d) BT458

RT-qPCR   Proliferation   Self-Renewal

-33.0% -20.5%

e) BT993

RT-qPCR   Proliferation   Self-Renewal

-21.8% -19.4%
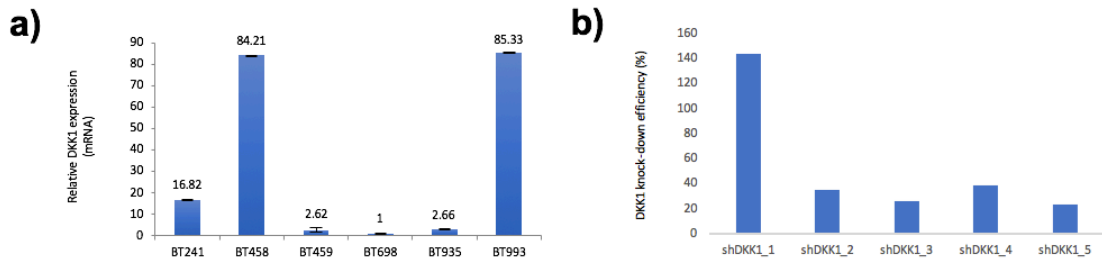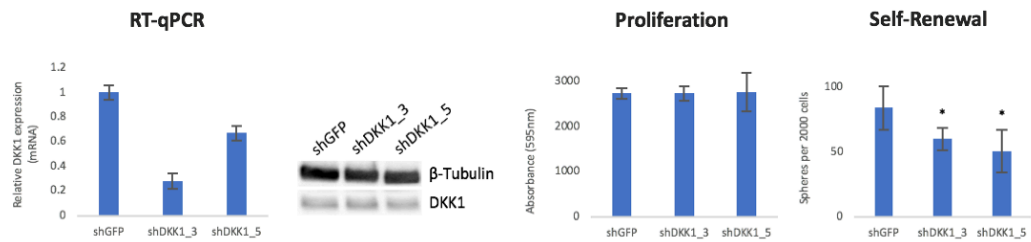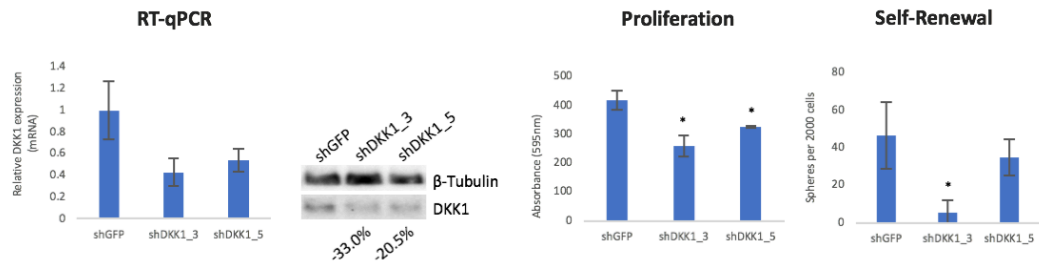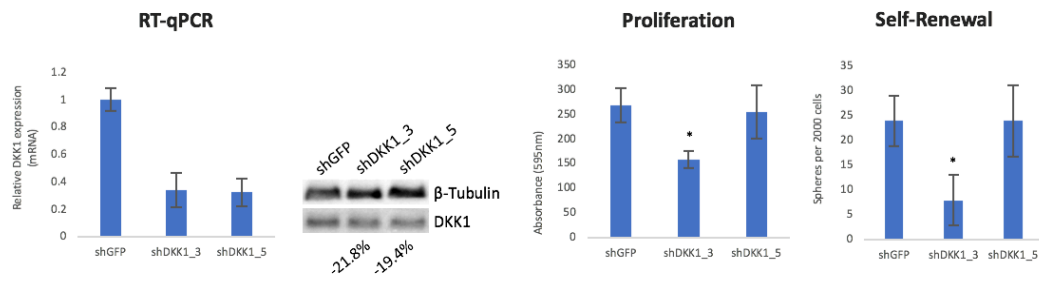
Figure 5. DKK1 maintains proliferation and self-renewal potential of patient-derived GBM. (**a**) BT241, BT458, and BT993 are identified as PDLs highly expressing DKK1. (**b**) shRNAs targeting DKK1 provided by the Moffat lab. The two most effective shRNAs tested in HAP1 cells were shDKK1_3 (74%) and shDKK1_5 (77%). (**c-e**) BT241, BT458, and BT993 were transduced with both selected shRNAs before gene and protein expressions of DKK1 were determined by RT-qPCR and western blotting, and the proliferation and self-renewal potentials determined as described. * designates a p-value < 0.05.

expression by 72.2% and 32.8%, but did not seem to affect protein levels (Figure 5c). The knock-down vectors were then used to test two key stem cell abilities; self-renewal and proliferation. As cancer stem cells are being studied, elucidating the effect of DKK1 on these cells' abilities to proliferate extensively and to retain their undifferentiated phenotype is crucial and commonplace in stemness studies. These knock-downs did not affect the proliferation of BT241s, but they did reduce their self-renewing potential by 28.6% (shDKK1_3) and 39.7% (shDKK1_5). It appears as if a more effective shRNA knock-down would be required for this cell line in order to affect its proliferation potential. It is curious however that none of the figures in Figure 5c correlate in terms of the largest knock-down leading to the largest decrease in functionality. shDKK1_3 offered the best mRNA knock-down, but shDKK1_5 offered the more effective reduction of self-renewal potential.

In BT458, the shDKK1_3 and shDKK1_5 decreased DKK1 gene expression by 57.1% and 46.1%, and protein expression by 33.0% and 20.5%, respectively (Figure 5d). BT458's rate of proliferation was affected by 37.6% (shDKK1_3) and 21.9% (shDKK1_5), which strongly correlates with its protein knock-downs. Its rate of self-renewal was decreased by 88.6% (shDKK1_3) and 25.7% (shDKK1_5). In contrary to the results obtained using BT241, the data does in fact correlate. Not only did shDKK1_3 once again grant the best transcription reduction, but it also reduced protein expression the most, and it negatively affected the proliferation and self-renewing potential of BT458 the most.

Finally in BT993, shDKK1_3 and shDKK1_5 decreased DKK1 gene expression by 65.8% and 67.3%, and protein expression by 21.8% and 19.4%, respectively (Figure 5e). Its rate of proliferation was diminished by 40.1% (shDKK1_3) and 4.9% (shDKK1_5)

while its rate of self-renewal was decreased by 66.7% by shDKK1_3, matching its transcriptional knock-down, but shDKK1_5 did not have an effect. Similarly to what was observed in the BT458 results, shDKK1_3 had the greatest functional effect on both the proliferation and self-renewal potential of BT993, however on the transcriptional and translational levels both shRNAs arguably had equivalent effects.

Anti-DKK1 mAb Blockade Experiments

In order to get a better understanding of DKK1's potential as a potential therapeutic target for GBM, we decided to attempt to hinder the proliferation and self-renewal potentials of GBM using an anti-DKK1 IgG mAb. This was done by incubating BT241 with two anti-DKK1 IgG mAbs produced by the Toronto Recombinant Antibody Centre (TRAC) as described (see Methods and Materials). TRAC demonstrated that both variants, #11516 and #11517, were shown to have dissociation constants (K_D) of 2.34 x 10^{-8} and 5.24 x 10^{-8}, respectively. It is also important to note these have not been validated for therapeutic usage, and the exact binding location of the antibodies on DKK1 is not currently known.

It was first decided to incubate BT241 with 200nM of each mAb (Figure 6a). This concentration was used because optimization by flow cytometry using commercial anti-DKK1 antibodies had failed and 200nM was chosen arbitrarily as a starting point based on previous work (discussed later). This first experiment demonstrated that clone #11516 of the anti-DKK1 IgG mAbs decreased the proliferation and self-renewal potentials of BT241
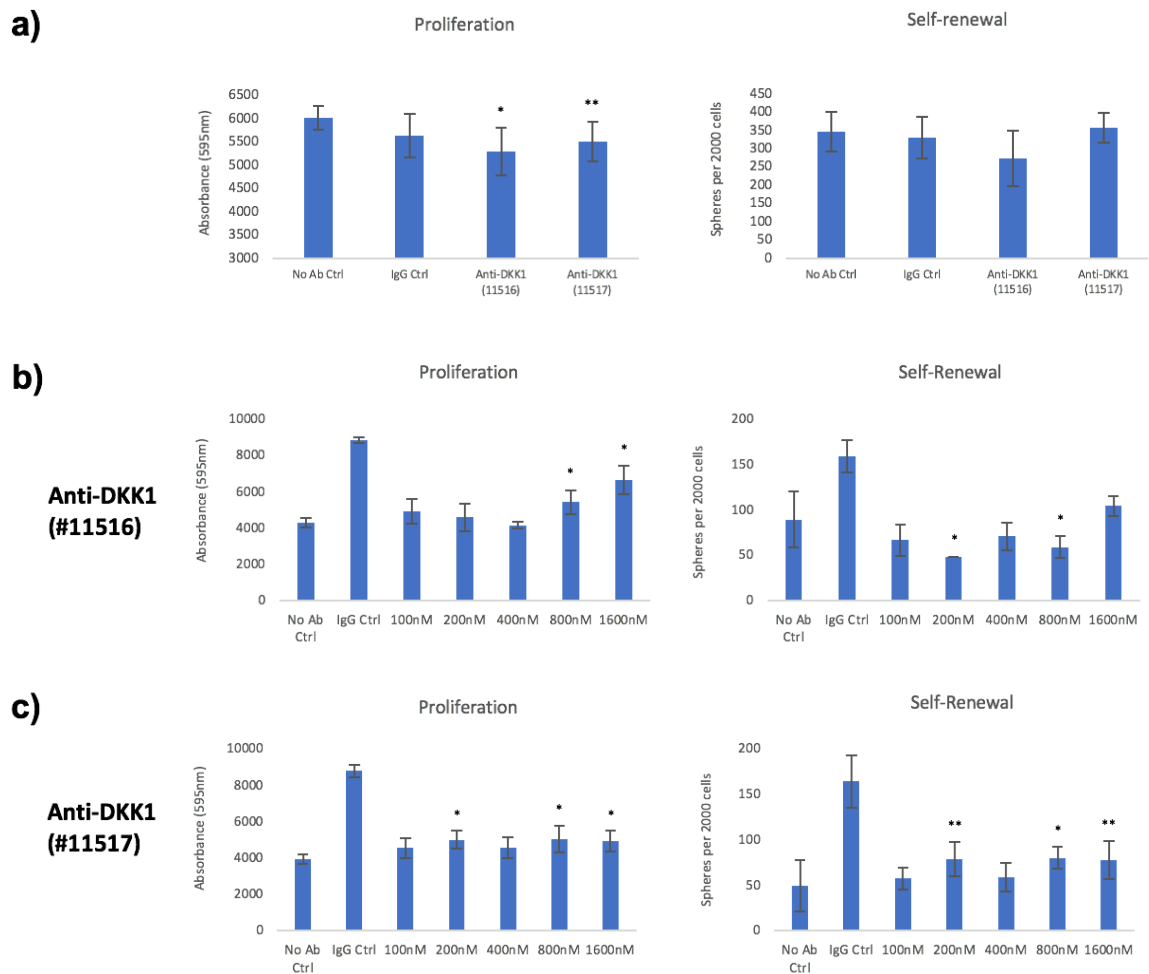
Figure 6. Effect of anti-DKK1 IgG monoclonal antibodies on glioblastoma proliferation and self-renewal. (**a**) BT241 cells treated with nothing (No Ab Ctrl), or 200nM of either an IgG isotype control mAb, or both anti-DKK1 IgG mAbs produced by TRAC. (**b-c**)) BT241 cells were treated with different concentrations of both variants of the anti-DKK1 IgG mAbs (#11516 and #11517) produced by TRAC. The absorbances of the proliferation assays were read at 595nm. All asterisks demonstrate the significance of the antibody effects in comparison to the no-antibody controls (No Ab Ctrl). Every sample

is significantly different from the IgG control. * designates a p-value < 0.05, and **

designates a p-value of < 0.1.

by 11.9% and 21.2%, respectively, whereas clone #11517 reduced proliferation by only 8.3% while self-renewal was unchanged.

To investigate whether 200nM was the optimal dose of antibodies, dose-response experiments were then performed using both antibody variants (Figure 6b, 6c). Interestingly, the two controls provided in each experiment did not match, as the IgG control increased both proliferation and self-renewal twofold or more compared to the no-antibody controls. In comparison to the no-antibody control, clone #11516 did not reduce the proliferation potential of BT241, and in fact the latter increased by 55.1% when incubated with the maximal concentration of 1600nM. The lowest values obtained were from the 200nM and 400nM concentrations in which proliferation was increased by 6.8% and decreased by 3.3% compared to the no-antibody control, respectively. In the self-renewal experiment, 200nM most successfully reduced BT241's potential by 46.2%. Similarly to the proliferation assay, incubating BT241 with 1600nM of variant #11516 increased self-renewal by 16.4%. Compared to the IgG control, proliferation was reduced by up to 53.04% (400nM) and self-renewal by up to 69.75% (200nM).

Using anti-DKK1 IgG mAb clone #11517 increased proliferation in each of the dosed samples compared to the no-antibody control, and no dose-dependent trend was noticed. Proliferation remained mostly unchanged regardless of concentration used, with the biggest and smallest changes coming from the 800nM (27.3% increase) and 100nM (15.1% increase) concentrations respectively, compared to the no-Ab control (Figure 6c). The self-renewal assay generated similar results, with self-renewal increasing in each anti-DKK1 samples compared to the no-antibody control, but once again with no noticeable

dose-dependent trend. The highest and lowest changes in self-renewal potential once again came from the 800nM (62% increase) and 100nM (16.2% increase), respectively. When compared to the IgG control, antibody variant #11517 reduced proliferation and self-renewal by up to 48.18% (100nM) and 65.04% (100nM), respectively

Another interesting observation is that the IgG control used increased both the proliferation and self-renewal potential of BT241 in all four experiments in comparison to every other dose (Figure 6b, 6c). This however was not observed in the 6a) panel. This could indicate that this IgG mAb may be having an effect, and may thus not be a proper control. On the contrary, it could indicate that the IgG control antibody is in fact a good control since the mere presence of antibodies may be having an effect. Hence it is important to quantify the effects of the anti-DKK1 antibodies in comparison to such a control. It is also very important to note that each of these experiments was only conducted once, and so they will need to be repeated, ideally with BT458 and BT993, before conclusions can be drawn. Since the results obtained in panel 6a differed from 6b and 6c, repeating the experiments again with BT241 would also be ideal.

All in all, these results seem to indicate that DKK1 has the potential to be a therapeutic target for GBM, however no solid conclusions can be drawn from the current data. To properly validate DKK1 as a therapeutic target for GBM, future experiments investigating DKK1's role on BTIC differentiation, and on downstream signalling of the canonical and non-canonical Wnt, and Akt pathways will be needed. The TRAC anti-DKK1 mAbs should be optimized for *in vitro* use before repeating the experiments with

BT241, BT458 and BT993. Afterwards, the mAbs will have to be tested *in vivo* by treating

mice bearing patient-derived tumours.

DISCUSSION

To start off, it is important to note that the research presented in Project 1 of this thesis is part of a large collaborative multidisciplinary research project involving three laboratories, the groups of Drs. Sheila Singh, Jason Moffat, and Sachdev Sidhu, and two additional organizations, the Toronto Recombinant Antibody Centre (TRAC) and the Centre for the Commercialization of Antibodies and Biologics (CCAB). The goal of the research project is aimed at the identification of targets of recurrent GBM and to develop corresponding antibody-based modalities. The Singh lab is responsible for establishing the PDX model and pipeline for sample acquisition and preparation for RNA-Seq. The RNA-Seq analysis is lead by the Moffat laboratory, and target identification is lead by the Singh lab. Antibody engineering is performed by the Sidhu lab, and the production is carried out by TRAC and CCAB. Finally, modality testing and validation is done by the Singh lab.

As alluded to, the first part of this project involved the establishment of a sample acquisition pipeline capturing the three main time-points in GBM progression using the most clinically relevant PDX mouse model of recurrent GBM we could generate in order to most accurately replicate clonal evolution and disease progression. A preliminary PDX model using PDL BTIC-based tumour spheres was previously developed by members of the Singh lab prior to my arrival. In order to make the model as clinically relevant as possible, we started by optimizing the chemotherapy dosing to replicate what patients go through in their therapy regimen by giving the mice equivalent levels of Temodal®

(clinical-grade TMZ) that patients receive orally, which is the therapeutic method of delivery. This means the dosage and delivery of the TMZ was identical to what patients receive. As previously mentioned, 50mg/kg of TMZ is equivalent to 150mg/m^2 according to FDA guidelines (Reagan-Shaw S, 2008). A meta-analysis and systematic review of TMZ in animal models also determined oral delivery was second only to intratumoural delivery in terms of survival and reduction of tumour burden (Hirst TC, 2013). With that being said, the model we use has a few drawbacks when it comes to mimicking the clinical treatment regimen. First off, the mice are only given 2Gy of whole-brain radiation once on the first day of treatment, in comparison to a daily dose of 2Gy for 30 days, which is what patients receive. This is the highest and most clinically relevant dose of brain radiation we were able to give consistently without unduly harming the mice. Previous work in the laboratory demonstrates that even though the level of radiation is much lower than what patients receive, the mice still gain a survival advantage from it. The data from Figure 2, and especially 2b, best demonstrates the significant effect that our chemoradiotherapy treatment has on tumour burden. A second drawback comes from the fact that human patients go through surgical resection of the bulk tumour mass prior to receiving chemotherapy and radiation. Unfortunately, we aren't able to perform such surgeries on immunocompromised mice due to high risk of infection and poor wound healing. Another minor drawback arises from our 2-week post-treatment MRD time-point. Two-weeks post-treatment was chosen as it seemed to be the best time at which the tumour burden is at its lowest, but we do not know this for a fact. As seen in Figure 2, each tumour reacts to treatment differently meaning they reach the point of MRD at different times. Time-course

experiments using each PDL could be conducted in order to determine the appropriate point of MRD for each line. Another, and perhaps the most important, of our model's drawbacks, arises from the immunodeficiency of the mice we use to create the PDX models – our model does not take into consideration immunological effects. This can have many effects on the tumour microenvironment, brain-related immune functions, the selection of tumour clones capable of evading the immune system, and more. This issue will become increasingly relevant when the project reaches the stage of testing the engineered immunotherapies in the PDX models. It should go without saying but testing immunotherapies on mice that do not have immune systems is problematic and leaves us with an incomplete view and understanding of the therapeutic, potentially synergistic, or negative side-effects of the therapy. The immune response will be especially important when validating therapies targeting DKK1 since the latter has previously been shown to play a role in the immune suppression of natural killer (NK) cells in latency competent cancer (LCC) (Malladi S, 2016), to inhibits macrophage and neutrophil recruitment in lung metastases (Zhuang X, 2017), to activate MDSCs (D'Amico L, 2016), and to block the secretion of pro-inflammatory cytokines (Fridman WH, 2012).

Moreover, another potential point of contention our model may generate is that it is a tumour sphere based PDX model. We chose this model type because they have been shown to have many advantages including retaining similar ITH and molecular profiles as well as being very phenotypically similar to that of the patient's original tumour (Lee J, 2006; Chen R, 2010; Günther HS, 2008; Wakimoto H, 2012). Previous work from the Singh laboratory has also demonstrated these same observations, indicating the patient's

original tumour is well modeled. Other well-known GBM models include PDXs using freshly biopsied tumour tissue, genetically engineered and syngeneic models. PDXs using freshly biopsied tumour tissue have the advantage of maintaining the architecture of the original tissue, including the endothelium, extracellular matrix, and tumour infiltrating immune cells (e.g. lymphocytes, macrophages) (Bjerkvig R, 1990), and syngeneic models can allow for an active immune system. However, the tremendous advantage of PDL tumour sphere PDX models like ours, in addition to the aforementioned, that far outweighs the listed drawbacks is the fact that we are able to make PDLs out of the patient tissue sample and extract more information per sample by being able to perform numerous experiments. A BTIC PDX model like ours also allows us to properly study GBM progression and clonal evolution based on the cancer stem cell model. Of course, an additional issue that arises from PDLs is that the tumour cells will change over time due to the accumulation of mutations and similar defects, and due to selection pressures emanating from the *in vitro* culturing process.

As previously mentioned, in order for our model to work, many things must go right. The patient tumour must survive being processed into a viable PDL, which must then be able to grow *in vitro* in serum-free NeuroCult™ media, it must be able to engraft and grow in a mouse host, it must respond to TMZ and radiation (it must enter remission), and finally the tumour must recur. This makes it very difficult to find GBM PDLs that will work. Each of these also present a number of selection pressures on the PDLs, meaning we may not be looking at the entire GBM population in our *in vitro* and *in vivo* experiments,

but perhaps merely a fraction of the total population – patients with tumours that have the cells able to survive and proliferate despite each mentioned selection pressure. Although our model is not perfect, it is a good starting point. Even if the targets discovered using this method only identifies proteins relevant to such a smaller population it is still crucial research, especially when taking into consideration the horrific conditions and uniformly fatal outcomes these patients face.

The degree of difficulty attached to finding GBM PDLs able to be used in our rGBM pipeline is best illustrated by the fact that until now only three PDLs (BT428, BT799, BT935) have provided us with meaningful data, and only two of these (BT428, BT935) have successfully gone through the pipeline (Figure 2). However, it seems to work considerably well as the tumour burden can be seen increasing in the control samples while the tumour significantly decreases in the samples treated with our chemoradiotherapy regimen, and the mice subsequently receive a very significant survival advantage. The three PDLs all reacted to the treatment differently, and recurred after significantly different times, further highlighting how some tumours are more resistant to therapy due to different cellular and molecular compositions. BT799 demonstrated the most drastic tumour reduction post-therapy in both the MRI scans and H&E stained tissue slides and was also the only tumour that did not recur. Other experiments performed using the same treatment regimen on the BT799 PDL, before and after this experiment, had the tumours relapse so why they did not in this case remains unknown. Although GBMs inevitably always relapse, some patients go years without having a recurrent tumour. It could be that the GBM was

59

indeed slowly recurring, but due to the short lifespan of the mice (typically 40-52 weeks), we were unable to see it happen. Nevertheless, in order to obtain the missing recurrent sample from BT799, the experiment will have to be repeated. Fortunately, we were successful in obtaining the MRD samples as this is what we believe to be the most crucial time-point of GBM progression since the point of this collaborative research project is to identify targets of the cells responsible for the recurrence of GBM. From a perhaps oversimplified clinical point-of-view, if we are able to use chemotherapy and radiation to kill the bulk tumour and add an additional therapy(ies) targeting the remaining cells, then we shouldn't have to worry about the tumour recurring.

The second project was also aimed at identifying novel markers of GBM had concerns of its own. Three samples did not pass quality control during the RNA-sequencing. This left us with only two biological replicates for the CD133+ GBM populations which is not enough samples to attain statistical significance. Although we continued with the experiment despite this unfortunate event, this should have been redone in order to have statistically significant results. Another flaw arose from the implicit presumption that CD133 is the exclusive marker of BTICs, which has been shown to not be the case. Although CD133 is the best studied and is thought to be the preeminent BTIC marker, others include CD15, ITGA6, L1CAM, EphA2, EphA3, and EphB2. This inherently means that, although the cells in the CD133+ GBM population are BTICs, the CD133- GBM populations are not rid of all BTICs and will contain some non-CD133 BTICs. The faulty assumption was done for experimental simplicity and feasibility, and

because CD133 is also a marker of NSCs. CD133 allowed for the simultaneous separation of BTICs from non-BTIC bulk tumour cells, and NSCs from NPCs and other downstream differentiated progenitors. This does however mean that the data obtained must be taken with a grain of salt as some upregulated genes in the CD133- GBM population may have been influenced from non-CD133 BTICs present in the population. Despite the uncertainties mentioned above, it is very encouraging to see that the top target identified in this screen was upregulated in one of two biological MRD samples. This serves not only to validate DKK1 as a candidate marker, but also to quell the said uncertainties.

Until now, the RNA-Seq samples shown in Figure 4 are all that have been sequenced so far although the recurrent samples of BT428 and BT935 have been obtained and snap-frozen. It would be ideal to send all samples from all time-points from all PDLs for RNA-sequencing at the same time to minimize unwanted sequencing errors and variations, but due to feasibility we decided to send the samples in batches to allow research project to proceed while more data pours in over time. Furthermore, although DKK1 was highly overexpressed in both CD133+ and CD133- GBM populations making it a target of GBM and not specifically GBM BTICs which was hoped, it remains a valid target to pursue. As DKK1 does not seem to be specific for BTICs, this would likely mean that it could not serve as a stand-alone target for the therapy-surviving GBM population. On the other hand, it remains possible that DKK1 is simply more highly overexpressed in that population than others as was seen in the BT428 experiment. It not being overexpressed in the MRD population of BT799 indicates that DKK1 might not be a universal GBM target

but may be more specific to a subset of GBMs. A study examining the relation between DKK1 and the four GBM subtypes and their recurrences, or any other given subset for that matter, would be interesting. In our data, only 30% (3/10) of the GBM PDLs tested turned out to highly express DKK1, so one could postulate that as a therapeutic target DKK1 may only be applicable to less than a third of patients. To bolster this claim, determining if DKK1 increases at MRD in BT458 and BT993 would be valuable. BT241, being a recurrent GBM PDL, will not be put through the rGBM pipeline established since the tumour has already survived and recurred after being treated with TMZ and radiation. Unfortunately, the patient-matched primary tumour of BT241 was not collected and so we cannot compare DKK1 levels in both. Moreover, the fact that BT428 had low levels of DKK1 pre-treatment indicates that DKK1 could be relevant to more than just primary tumours highly expressing DKK1. In order for such information to be useful clinically, efforts should be made to identifying a molecular signature. Such would be crucial in predicting in which patients DKK1 could be expected to select for the population of cells capable of surviving standard therapy.

Moving on to the validation of DKK1 as a potential target of GBM, the results obtained between the three PDLs demonstrated that inhibiting DKK1 can reduce the proliferation and self-renewal capabilities of GBM. However, the results obtained were not consistent. BT241's proliferation remained unaffected by DKK1 suppression. Also, in the functional assays shDKK1_3 seemed to have a greatest effect of the two shRNAs with the exception of BT241's self-renewal assay where shDKK1_5 was more effective.

These differences in functionality suggests there are inherent differences between tumours and that they are not necessarily all equally driven by the same proteins.

An interesting observation was that knocking-down DKK1 in BT241 did not seem to lower its protein expression levels, and despite this its self-renewal was still affected. A similar effect can be noticed in the BT993 samples, as both shDKK1s are shown to have essentially equivalent effects, but only shDKK1_3 is shown to have a functional effect. The reason for that is the data from the RT-qPCR, western blots, and proliferation and self-renewal assays are not from the same experiment. However, these were chosen as this was the trend that was consistently seen across the majority of samples. These assays should be replicated with BT241 and BT993 in order to have the entire panel originating from the same experiment. In the case of BT458, everything went according to plan. The knock-downs reduced mRNA levels, protein levels, proliferation, and self-renewal in similar fashions, and shDKK1_3 was decidedly the more functionally effective shRNA. In order to see bigger functional effects, using multiple shRNAs simultaneously, or using CRISPR knock-outs might be preferable.

Moving forward in the validation of DKK1 as a target of GBM, it will be important to test its effect on differentiation, the only core stemness property not yet tested on the GBM PDLs. DKK1 has previously been shown to prevent the differentiation of osteosarcoma cells, promoting a CSC phenotype (Krause U, 2014; Goldstein SD, 2016), thus it could be expected that suppressing DKK1 expression via short-hairpin knock-down would increase the rate of differentiation of our GBM PDLs. Understanding of DKK1's

potential promotion of a CSC phenotype would be crucial in GBM research. GBM is well known to display high levels of anaplasia (poor cellular differentiation) and BTICs are known to be resistant to both chemotherapy and radiation (Louis DN, 2016; Liu G, 2006; Chen S, 2011; Bao S, 2006) meaning DKK1 could play a central role in GBM progression and recurrence. If CSC are indeed the driving force behind GBM, finding a way to reduce this population by triggering differentiation would be an avenue worth exploring.

In the final stage of this project, our collaborators in the Sidhu laboratory along with the TRAC and CCAB designed, engineered and produced human anti-DKK1 monoclonal IgG antibodies, as the end goal of the collaborative project is to make and validate immunotherapies targeting the candidates identified via various screens, of which the RNA-Seq analyses mentioned in this thesis are included. Since DKK1 is a secreted protein, the decision to select an IgG mAb as the modality of choice was an easy one to make as the other types of immunotherapies, like BiTEs or CAR T cells, are meant to target surface proteins. Our rationale was also confirmed by the fact that the only clinical antibody modalities used to target DKK1 are IgG mAbs. BHQ880 and DKN-01, owned by Novartis and Leap Therapeutics, are both being investigated in various phase I and phase II clinical trials for a wide range of cancers not including GBM.

Prior to testing the antibodies as seen in Figure 6, attempts to find out what the ideal concentration to use to see an effect in vitro were unsuccessful. We tried using a commercial anti-DKK1 antibody for flow cytometry in an attempt to determine the amount of DKK1+ cells in a given population. Our rationale was to determine the DKK1 positivity

of a given GBM PDL, and then use the TRAC antibodies in a dose-response manner to match the results obtained with the commercial antibody. For example, if BT241 would have been shown to be 70% positive using the commercial antibody, we would have tried different doses of the TRAC antibodies to find out what amount is needed to obtain the same results. However, the issue that arose was that every PDL tested with both the commercial and the TRAC antibodies came back nearly 100% positive for DKK1. Tests were also performed using PDLs that had been shown to have low expressions of DKK1 (i.e. BT698, BT935) and using shDKK1 knock-downs. The reason for this is thought to be due to two main reasons. First DKK1 is an important member of the ubiquitous Wnt pathway, so perhaps virtually every cell did in fact express DKK1 which would not be such a surprise considering canonical Wnt is known to be active in GBM (Sandberg CJ, 2013; Kaur N, 2013; Schule R, 2012). The second reason is that DKK1 is a secreted protein, meaning that it is present in the media with all other GBM cells and that it can bind any cell thus making them all appear as false-positives by FACS. Going forward, a potential way to resolve this issue could be to use CRISPR knock-outs to rid cells of the gene since shRNA only reduce expression at best (positive cells will remain positive for DKK1).

With the roadblock in mind, we decided to proceed with TRAC antibodies and attempt to treat *in vitro* cultures to discover whether the antibodies had therapeutic potential. In need of a starting point, we decided to start with a concentration of 200nM based on previous work done in the laboratory with other antibodies manufactured by TRAC. The initial results seemed to indicate these antibodies had some potential, so we proceeded to perform a dose-response experiment going all the way up to a concentration

of 1600nM. Unfortunately, the results weren't as promising. The most peculiar observation is the fact that the two controls used gave very different results in the b) and c) panels. In comparison to the cells without any control antibody, proliferation and self-renewal seemed either unaffected or even positively impacted by the presence of the anti-DKK1 antibodies. However, in comparison to the IgG isotype control, both proliferation and self-renewal were significantly reduced. This could indicate that the mere physical presence of an IgG antibody, even if it should not theoretically bind anything, has an effect on proliferation and self-renewal perhaps due to non-specific binding. With that being said, it is very important to note that each of the experiments illustrated by Figure 6 were only performed once, and only with BT241. As was seen on Figure 5, different PDLs react differently to DKK1 expression, and BT241 was actually the PDL that reacted the least to DKK1 knock-down. Another important factor that we did not yet test for is the possibility that, since DKK1 is a secreted protein, the antibodies may have been depleted and thus had little effect. The cells were incubated with the stated concentration of antibodies for a period of four days before the data was read out, so perhaps periodically supplementing the cultures with additional antibodies, or changing the media altogether, would allow us to see greater functional effects.

DKK1 presents an interesting target for GBM for many reasons. It is mainly thought of as a secreted inhibitor of canonical Wnt signalling, a highly relevant and ubiquitous pathway in oncology as Wnt expression has often been shown to be overly active in many different forms of cancer, including GBM. This led many to believe DKK1

to be a tumour suppressor, which it has been shown to be in some cases, but it has been shown promote cancer growth or be highly expressed in many other cancers (Kagey MH, 2017). There have also been contradicting studies of DKK1 in the context of gliomas demonstrating both the hypermethylation of DKK1 (Gotze S, 2010), and high CSF levels of DKK1 correlating with malignancy and increased classification (Zhou Y, 2010). A number of Wnt activators and repressors are being investigated in the context of GBM in clinical trials and in pre-clinical models, further demonstrating the lack of comprehension with regard to Wnt signalling in GBM (Suwala AK, 2016). Altogether, these studies indicate that the role of DKK1 is highly cancer-type dependent, and perhaps also dependent on other factors affecting its role even within cancer types like GBM. It is also for these reasons that previous studies and conclusions of DKK1's role in other cancers cannot be extrapolated to GBM.

Complicating things one step further is the fact that the mechanism by which DKK1 may be promoting cancer development is not understood. A number of mutations leading to the constitutive accumulation and activation of β-catenin signalling such as loss-of-function mutations in APC (destruction complex) and ZNRF3/RNF43 (ubiquitin ligases targeting FZD), and β-catenin-stabilizing mutations have been found in numerous cancers (*i.e.* colorectal, liver, endometrioid and others), but none have been found in GBM. In addition, β-catenin-independent Wnt signalling has also been implicated in promoting cancer (Sedgwick AE, 2016; Wang, 2009; Katoh, 2005), and DKK1 has been involved in the activation of this pathway as well in liver, prostate, ovarian and osteosarcoma cancers (Tao YM, 2013; Thudi NK, 2011; Wang S, 2011; Krause U, 2014). The only known

mutations related to the Wnt pathway in GBM are in proteins mainly related to suppressing it. These include mutations in WIF-1, which binds the Wnt ligands and stops it from activating the pathway (Yang Z, 2010; Lambiv WL, 2011), FAT1, which binds β-catenin to stop its translocation to the nucleus (Morris LG, 2013), and PEG3, which degrades β-catenin (Jiang X, 2010).

Crucial to the continuation of this project is determining in what capacity DKK1 signals through both the β-catenin and β-catenin-independent Wnt pathways. In order to quantify canonical Wnt activity, β-catenin reporter assays such as the luciferase-based TopFlash assay can be combined with functional knock-downs (or knock-outs) to read out β-catenin activity with or without DKK1 expression. β-catenin-independent signalling activity in GBM could be determined by measuring the phosphorylation levels of JNK, a downstream target of this pathway commonly used to measure the pathway's activation.

An interesting aspect emanating from DKK1 being a GBM target is the fact that, at first glance, it seems counterintuitive. DKK1, through negative feedback, self-regulates as it is itself a target of the TCF/LEF transcription factors. So as β-catenin Wnt signalling increases, so does DKK1 to keep the pathway from being overexpressed. How can β-catenin activity and DKK1 simultaneously be highly expressed if no known mutations in the Wnt pathway in GBM explain it? The answer may lie in a recent discovery. Canonical Wnt and Akt crosstalk has been well documented for some time as Akt has been shown to activate canonical Wnt via the phosphorylation and inhibition of GSK3 (Cross DA, 1995). However, the missing link that could explain the phenomenon is a discovery that has

expanded the known role of DKK1 and identified cytoskeleton associated protein 4 (CKAP4) as a novel DKK1 receptor. Through this interaction, it was demonstrated that DKK1 signalling is able to activate Akt via CKAP4 (Kimura H e. a., 2016). High DKK1 expression could thus potentially activate Akt/PI3K signalling through CKAP4, increasing β-catenin/Wnt signalling through the inhibition of GSK3 (Figure 7). It would be interesting to see if this could be shown to be the case in GBM through coupling the immunoblotting of Akt and GSK3 with a β-catenin reporter assay.

The work presented in this thesis demonstrated the successful optimization of a PDX model for rGBM, the establishment of a sample-acquisition pipeline of GBM progression, and the identification of DKK1 as a novel potential therapeutic target of GBM via two transcriptomic profiling screens. DKK1 was then successfully shown to be important in the maintenance of stemness properties of GBM BTICs like proliferation and self-renewal. The preliminary results obtained by attempting to block DKK1 signalling using IgG mAbs did not appear promising, but they were only tested on one PDL and their proper dosing has not yet been optimized. As discussed above, there are a number of experiments that will need to be conducted in order to properly validate DKK1 as a therapeutic candidate for GBM, and the data presented in this thesis will serve as the foundation going forward.
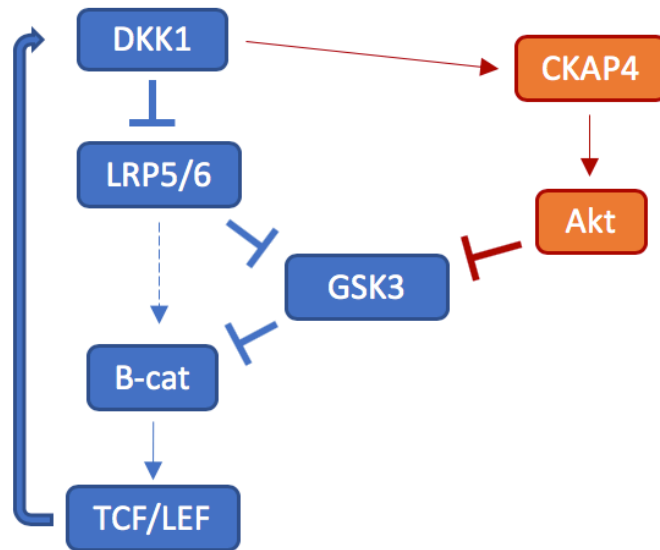
Figure 7. Proposed DKK1-Akt-β-catenin signalling model. Simultaneous high DKK1 expression and highly active canonical Wnt signalling (blue) may be explained by the additional activation of Akt by DKK1 via CKAP4 (orange). This signalling model remains untested.

REFERENCES

Abdouh M, et al. (2009). BMI1 sustains human glioblastoma multiforme stem cell renewal. *J Neurosci, 29*, 8884-96.

Ahn VE, et al. (2011). Structural basis ofWnt signaling inhibition by Dickkopf binding to LRP5/6. *Dev Cell, 21*, 862-73.

Al Hajj M, et al. (2003). Prospective identification of tumorigenic breast cancer cells. *PNAS, 100*(7), 3983-8.

Bao J, et al. (2012). The structural basis of DKK-mediated inhibition of Wnt/LRP signaling. *Sci Signal, 5*, pe22.

Bao S, et al. (2006). Glioma stem cells promote radioresistance by preferential activation of the DNA damage response. *Nature, 444*(7120), 756-60.

Bao S, et al. (2008). Targeting cancer stem cells through L1CAM suppresses glioma growth . *Cancer Res, 68*, 6043-8.

Beier D, et al. (2012). Efficacy of clinically relevant temozolomide dosing schemes in glioblastoma cancer stem cell lines. *J Neurooncol, 109*(1), 45-52.

Binda E, et al. (2012). The EphA2 receptor drives self-renewal and tumorigenicity in stem-like tumor-propagating cells from human glioblastomas. *Cancer Cell, 22*(6), 765-80.

Bjerkvig R, et al. (1990). Multicellular tumor spheroids from human gliomas maintained in organ culture. *J Neurosurg, 72*(3), 463-75.

Bonnet D, et al. (1997). Human acute myeloid leukemia is organized as a hierarchy that originates from a primitive hematopoietic cell. *Nature Med, 3*(7), 730-7.

Bourdon MA, et al. (1984). Monoclonal antibody localization in subcutaneous and intracranial human glioma xenografts: paired-label and imaging analysis. *Anticancer Res, 4*(3), 133-40.

Bourhis E, et al. (2011). Wnt antagonists bind through a short peptide to the first betapropeller domain of LRP5/6. *Structure, 19*, 1433-42.

Bullain SS, et al. (2009). Genetically engineered T cells to target EGFRvIII expressing glioblastoma . *J Neurooncol, 94*(3), 373-82.

Burrell R, et al. (2013). The causes and consequences of genetic heterogeneity in cancer evolution. *Nature, 501*, 338-45.

Chen J, et al. (2012). A restricted cell population propagates glioblastoma growth after chemotherapy. *Nature, 488*(7412), 522-6.

Chen R, et al. (2010). A hierarchy of self-renewing tumor-initiating cell types in glioblastoma. *Cancer Cell, 17*(4), 362-75.

Chen S, et al. (2011). Structural and functional studies of LRP6 ectodomain reveal a platform for Wnt signaling. *Dev Cell, 21*, 848-61.

Cheng Z, et al. (2011). Crystal structures of the extracellular domain of LRP6 and its complex with DKK1. *Nat Struct Mol Biol, 18*, 1204-10.

Choi BD, et al. (2013). Regulatory T cells are redirected to kill glioblastoma by an EGFRvIII-targeted bispecific antibody. *Oncoimmunology, 2*(12), e26757.

Cross DA, et al. (1995). Inhibition of glycogen synthase kinase-3 by insulin mediated by

protein kinase B. *Nature, 378*(6559), 785-9.

Day BW, et al. (2013). phA3 maintains tumorigenicity and is a therapeutic target in

glioblastoma multiforme. *Cancer Cell, 23*(2), 238-48.

D'Amico L, et al. (2016). Dickkopf-related protein 1 (Dkk1) regulates the accumulation

and function ofmyeloid derived suppressor cells in cancer. *J Exp Med*, 213: 827–

840.

Fasano CA, et al. (2007). shRNA knockdown of Bmi-1 reveals a critical role for p21-Rb

pathway in NSC self-renewal during development. *Cell Stem Cell, 1*, 87-99.

Favero. (2015). Glioblastoma adaptation traced through decline of an IDH1 clonal driver

and macro-evolution of a double-minute chromosome. *Ann Oncol, 26*(5), 880-7.

Fridman WH, et al. (2012). The immune contexture in human tumours: impact on clinical

outcome. *Nature Rev Cancer*, 12: 298–306.

Günther HS, et al. (2008). Glioblastoma-derived stem cell-enriched cultures form distinct

subgroups according to molecular and phenotypic criteria. *Oncogene, 27*(20),

2897–909.

Gedeon PC, et al. (2014). An EGFRvIII-targeted bispecific T-cell engager overcomes

limitations of the standard of care for glioblastoma. *Expert Rev Clin Pharmacol,

6*(4), 375-86.

Goldstein SD, et al. (2016). A monoclonal antibody against the Wnt signaling inhibitor

dickkopf-1 inhibits osteosarcoma metastasis in a preclinical model. *Oncotarget*, 7:

21114–21123.

Gotze S, et al. (2010). Frequent promoter hypermethylation of Wnt pathway inhibitor genes in malignant astrocytic gliomas. *Int J Cancer, 126*(11), 2584-93.

Graham V, et al. (2003). SOX2 functions to maintain neural progenitor identity . *Neuron, 39*, 749-65.

Green J, et al. (2014). The role of Ryk and Ror receptor tyrosine kinases in Wnt signal transduction. *Cold Spring Harb Perspect Biol, 6*, 1-12.

Hirata H, et al. (2009). Wnt antagonist gene DKK2 is epigenetically silenced and inhibits renal cancer progression through apoptotic and cell cycle pathways. *Clin Cancer Res, 15*(18), 5678-87.

Hirst TC, et al. (2013). Systematic review and meta-analysis of temozolomide in animal models of glioma: was clinical efficacy predicted? *Br J Cancer, 108*(1), 64-71.

Huse JT, et al. (2010). Targeting brain cancer: advances in the molecular pathology of malignant glioma and medduloblastoma. *Nat Rev Cancer, 10*(5), 319-31.

Jiang X, et al. (2010). The imprinted gene PEG3 inhibits Wnt signaling and regulates glioma growth. *J Biol Chem, 285*(11), 8472-80.

Johnson BE, et al. (2014). Mutational analysis reveals the origin and therapy-driven evolution of recurrent glioma. *Science, 343*(6167), 189-93.

Johnson LA, et al. (2015). Rational development and characterization of humanized anti–EGFR variant III chimeric antigen receptor T cells for glioblastoma. *Sci Transl Med, 7*(275), 275ra22.

Kagey MH, and He X (2017). Rationale for targeting the Wnt signalling modulator Dickkopf-1 for oncology. *Br J Pharmacol, 174*(24), 4637-4650.

Kaneko Y, et al. (2000). Musashi1: an evolutionally conserved marker for CNS

    progenitor cells including neural stem cells . *Dev Neurosci, 22*, 139-53.

Katoh, M. (2005). WNT/PCP signaling pathway and human cancer (review). *Oncol Rep,*

    14, 1583-8.

Kaur N, et al. (2013). Wnt3a mediated activation of Wnt/ b-catenin signaling promotes

    tumor progression in glioblastoma. *Mol Cell Neurosci, 54*, 44-57.

Kim H, et al. (2015). Whole-genome and multisector exome sequencing of primary and

    post-treatment glioblastoma reveals patterns of tumor evolution. *Genome Res,*

    25(3), 316-27.

Kim J, et al. (2015). Spatiotemporal Evolution of the Primary Glioblastoma Genome.

    Cancer Cell, 28(3), 318-28.

Kimura H, et al. (2016). CKAP4 is a Dickkopf1 receptor and is involved in tumor

    progression. *J Clin Invest, 126*(7), 2689-705.

Kochenderfer JN, et al. (2015). Chemotherapy-refractory diffuse large B-cell lymphoma

    and indolent B-cell malignancies can be effectively treated with autologous T

    cells expressing an anti-CD19 chimeric antigen receptor. *J Clin Oncol, 33*(6), 540-

    9.

Kong S, et al. (2012). Suppression of human glioma xenografts with second-generation

    IL13R-specific chimeric antigen receptor-modified T cells. *Clin Cancer Res,*

    18(21), 5949-60.

Krause U, et al. (2014). An unexpected role for a Wnt-inhibitor: Dickkopf-1 triggers a

   novel cancer survival mechanism through modulation of aldehyde-

   dehydrogenase-1 activity. *Cell Death Dis, 5*, e1093.

Krause U, et al. (2014). An unexpected role for a Wnt-inhibitor: Dickkopf-1 triggers a

   novel cancer survival mechanism through modulation of aldehyde-

   dehydrogenase-1 activity. *Cell Death Dis, 5*, e1093.

Lambiv WL, et al. (2011). The Wnt inhibitory factor 1 (WIF1) is targeted in glioblastoma

   and has a tumor suppressing function potentially by induction of senescence.

   Neuro Oncol, 13(7), 736-47.

Lathia JD, et al. (2010). Integrin alpha 6 regulates glioblastoma stem cells . *Cell Stem

   Cell, 6*, 421-32.

Lee J, et al. (2006). Tumor stem cells derived from glioblastomas cultured in bFGF and

   EGF more closely mirror the phenotype and genotype of primary tumors than do

   serum-cultured cell lines. *Cancer Cell, 9*(5), 391-403.

Liu G, et al. (2006). Analysis of gene expression and chemoresistance of CD133+ cancer

   stem cells in glioblastoma. *Mol Cancer, 5*, 67.

Louis DN, et al. (2007). The 2007 WHO classification of tomours of the central nervous

   system. *Acta Neuropathol, 114*(2), 97-109.

Louis DN, et al. (2016). The 2016 World Health Organization Classification of Tumors of

   the Central Nervous System: a summary. *Acta Neuropathol, 131*(6), 803-20.

Malladi S, et al. (2016). Metastatic latency and immune evasion through autocrine

   inhibition of WNT. *Cell*, 165: 45–60.

Manoranjan B, et al. (2013). FoxG1 Interacts with Bmi1 to Regulate Self-Renewal and

    Tumorigenicity of Medulloblastoma Stem Cells . *Stem Cells, 31*, 1266-77.

Mao B, et al. (2003). Kremen2 modulates Dickkopf2 activity during Wnt/LRP6 signaling.

    Gene, 302(1-2), 179-83.

Matoba K, et al. (2017). Conformational freedom of the LRP6 ectodomain Is regulated by

    N-glycosylation and the binding of the Wnt antagonist Dkk1. *Cell Rep, 18*, 32-40.

Maude SL, et al. (2014). Chimeric antigen receptor T cells for sustained remissions in

    leukemia. *N Engl J Med, 371*(16), 1507-17.

Mazon M, et al. (2016). Modulating Dickkopf-1: a strategy to monitor or treat cancer?

    Cancers (Basel), 8: 1-16.

Meacham CE, et al. (2013). Tumour heterogeneity and cancer cell plasticity. *Nature, 501*,

    328-37.

Meyer M, et al. (2015). Single cell-derived clonal analysis of human glioblastoma links

    functional and genomic heterogeneity. *PNAS, 112*(3), 851-6.

Miao H, et al. (2014). EGFRvIII-specific chimeric antigen receptor T cells migrate to and

    kill tumor deposits infiltrating the brain parenchyma in an invasive xenograft

    model of glioblastoma. *PLoS One, 9*(4), e94281.

Mohammadpour H, et al. (2016). Key role of Dkk3 protein in inhibition of cancer cell

    proliferation: An in silico identification. *J Theor Biol, 393*, 98-104.

Morgan RA, et al. (2012). Recognition of glioma stem cells by genetically modified T

    cells targeting EGFRvIII and development of adoptive cell therapy for glioma.

    Hum gene Ther, 23(10), 1043-53.

Morris LG, et al. (2013). Recurrent somatic mutation of FAT1 in multiple human cancers leads to aberrant Wnt activation. *Nat Genet, 45*(3), 253-61.

Murat A, et al. (2008). Stem Cell-Related 'Self-Renewal' Signature and High Epidermal Growth Factor Receptor Expression Associated With Resistance to Concomitant Chemoradiotherapy in Glioblastoma. *J Clin Oncol, 26*, 2015-24.

Nakada M, et al. (2010). The phosphorylation of ephrin-B2 ligand promotes glioma cell migration and invasion. *Int J Cancer, 126*(5), 1155-65.

Nakamura RE, et al. (2010). Analysis of Dickkopf3 interactions with Wnt signaling receptors. *Growth Factors, 28*(4), 232-42.

Notta F, et al. (2011). Evolution of human BCR-ABL1 lymphoblastic leukemia-initiating cells. *Nature, 469*, 362-67.

Ohgaki H, et al. (2005). Epidemiology and etiology of gliomas. *Acta Neuropathol, 109*(1), 93-108.

Ouyang Y, et al. (2016). Transcriptomic changes associated with DKK4 overexpression in pancreatic cancer cells detected by RNA-Seq. *Tumour Biol, 37*(8), 10827-38.

Pastrana E, et al. (2011). Eyes wide open: a critical review of sphere-formation as an assay for stem cells. *Cell Stem Cell, 8*(5), 486-98.

Patel AP, et al. (2014). Single-cell RNA-seq highlights intratumoral heterogeneity in primary glioblastoma. *Science, 344*(6190), 1396-1401.

Porter DL, et al. (2011). Chimeric antigen receptor-modified T cells in chronic lymphoid leukemia. *N Engl J Med, 365*(8), 725-33.

Ramaswamy V, et al. (2015). The Amazing and Deadly Glioma Race. *Cancer Cell, 28*(3), 275-7.

Reagan-Shaw S, et al. (2008). Dose translation from animal to human studies revisited. *FASEB J*, 22(3): 659-61.

Reinartz R, et al. (2017). Functional subclone profiling for prediction of treatment-induced intratumor population shifts and discovery of rational drug combinations in human glioblastoma. *Clin Cancer Res, 23*(2), 562-74.

Rheinbay E, et al. (2013). An aberrant transcription factor network essential for Wnt signaling and stem cell maintenance in glioblastoma. *Cell Rep, 3*(5), 1567-79.

Sampson JH, et al. (2014). EGFRvIII mCAR-modified T-cell therapy cures mice with established intracerebral glioma and generates host immunity against tumor-antigen loss. *Clin Cancer Res, 20*(4), 972-84.

Sandberg CJ, et al. (2013). Comparison of glioma stem cells to neural stem cells from the adult human brain identifies dysregulated Wnt-signaling and a fingerprint associated with clinical outcome. *Exp Cell Res, 319*, 2230-43.

Schule R, et al. (2012). Potential canonical wnt pathway activation in high-grade astrocytomas. *Sci World J, 2012*, 697313.

Scorsetti M, et al. (2015). Multimodality therapy approaches, local and systemic treatment, compared with chemotherapy alone in recurrent glioblastoma. *BMC Cancer, 15*(486).

Scott AM, et al. (2007). A phase I clinical trial with monoclonal antibody ch806 targeting transitional state and mutant epidermal growth factor receptors. *PNAS, 104*(10), 4071-6.

Sedgwick AE, et al. (2016). Wnt signaling in cell motility and invasion: drawing parallels between development and cancer. *Cancers (Basel), 8*, 1-15.

Shao YC, et al. (2017). The role of Dickkopf family in cancers: from Bench to Bedside. *Am J Cancer Res, 7*(9), 1754-68.

Shcherbakova DM, et al. (2013). Near-infrared fluorescent proteins for multicolor in vivo imaging. *Nature Methods, 10*(8), 751-4.

Shi RY, et al. (2013). High expression of Dickkopf-related protein 1 is related to lymphatic metastasis and indicates poor prognosis in intrahepatic cholangiocarcinoma patients after surgery. *Cancer*, 119: 993–1003.

Singh SK, et al. (2003). Identification of a cancer stem cell in human brain tumors. *Cancer Res, 63*(18), 5821-8.

Singh SK, et al. (2004). Identification of human brain tumour initiating cells. *Nature, 432*(7015), 396-401.

Son MJ, et al. (2009). SSEA-1 is an enrichment marker for tumor-initiating cells in human glioblastoma . *Cell Stem Cell, 4*, 440-52.

Sottoriva A, et al. (2013). Intratumor heterogeneity in human glioblastoma reflects cancer evolutionary dynamics. *PNAS, 110*(10), 4009-14.

Stupp R, et al. (2005). Radiotherapy plus Concomitant and Adjuvant Temozolomide for Glioblastoma. *N Engl J Med, 352*, 987-996.

Suryadevara CM, et al. (2015). Are BiTEs the "missing link" in cancer therapy? . *Oncoimmunology, 4*(6), e1008339.

Suva ML, et al. (2014). Reconstructing and reprogramming the tumor-propagating potential of glioblastoma stem-like cells . *Cell, 157*, 580-94.

Suwala AK, et al. (2016). Clipping the Wings of Glioblastoma: Modulation of WNT as a Novel Therapeutic Strategy. *J Neuropathol Exp Neurol, 75*(5), 388-96.

Swanton, C. (2015). Cancer evolution constrained by mutation order. *N Engl J Med, 372*, 661-63.

Szerlip NJ, et al. (2012). Intratumoral heterogeneity of receptor tyrosine kinases EGFR and PDGFRA amplification in glioblastoma defines subpopulations with distinct growth factor response. *PNAS, 109*(8), 3041-6.

Tao YM, et al. (2013). Dickkopf-1 (DKK1) promotes invasion and metastasis of hepatocellular carcinoma. *Dig Liver Dis, 45*, 251-7.

Thudi NK, et al. (2011). Dickkopf-1 (DKK-1) stimulated prostate cancer growth and metastasis and inhibited bone formation in osteoblastic bone metastases. *Prostate, 71*, 615-25.

Till BG, et al. (2012). CD20-specific adoptive immunotherapy for lymphoma using a chimeric antigen receptor with both CD28 and 4-1BB domains: pilot clinical trial results. *Blood, 119*(17), 3940-50.

Uchida N, et al. (2000). Direct isolation of human central nervous system stem cells. *PNAS, 97*(26), 14720-5.

Venugopal C, et al. (2012). Bmi1 marks intermediate precursors during differentiation of human brain tumor initiating cells. *Stem Cell Res, 8*, 141-53.

Venugopal C, et al. (2015). Pyrvinium Targets CD133 in Human Glioblastoma Brain Tumor-Initiating Cells. *Clin Cancer Res, 21*(23), 5324-37.

Verhaak R, et al. (2010). Integrated genomic analysis identifies clinically relevant subtypes of glioblastoma characterized by abnormalities in PDGFRA, IDH1, EGFR, and NF1. *Cancer Cell, 17*(1), 98-110.

Wakimoto H, et al. (2012). Maintenance of primary tumor phenotype and genotype in glioblastoma stem cells. *Neuro Oncol, 14*(2), 132-44.

Wang S, et al. (2011). Dickkopf-1 is frequently overexpressed in ovarian serous carcinoma and involved in tumor invasion. *Clin Exp Metastasis, 28*, 581-91.

Wang Y, et al. (2013). GSK3β/β-catenin signaling is correlated with the differentiation of glioma cells induced by wogonin. *Toxicol Lett, 222*(2), 212-23.

Wang, Y. (2009). Wnt/planar cell polarity signaling: a new paradigm for cancer therapy. *Mol Cancer Ther, 8*, 2103-9.

Wechsler-Reya R, et al. (2001). The developmental biology of brain tumours. *Annu Rev Neurosci, 21*(1), 385-428.

Wei W, et al. (2016). Single-Cell Phosphoproteomics Resolves Adaptive Signaling Dynamics and Informs Targeted Combination Therapy in Glioblastoma. *Cancer Cell, 29*(4), 563-73.

Yamabuki T, et al. (2007). Dikkopf-1 as a novel serologic and prognostic biomarker for lung and esophageal carcinomas. *Cancer Res*, 67: 2517–2525.

Yang Z, et al. (2010). Downregulation of WIF-1 by hypermethylation in astrocytomas. *Acta Biochim Biophys Sin (Shanghai), 42*(6), 418-25.

Zagzag D, et al. (2005). Downregulation of major histocompatibility complex antigens in invading glioma cells: stealth invasion of the brain. *Lab Invest, 85*(3), 328-41.

Zalutsky MR, et al. (1989). Pharmacokinetics and tumor localization of 131I-labeled anti-tenascin monoclonal antibody 81C6 in patients with gliomas and other intracranial malignancies. *Cancer Res, 49*(10), 2807-13.

Zhou Y, et al. (2010). Analysis of the expression profile of Dickkopf-1 gene in human glioma and the association with tumor malignancy. *J Exp Clin Cancer Res, 29*(138).

Zhu Y, et al. (2002). The molecular and genetic basis of neurological tumours. *Nat Rev Cancer, 2*(8), 616-26.

Zhuang X, et al. (2017). Differential effects on lung and bone metastasis of breast cancer by Wnt signalling inhibitor DKK1. *Nat Cell Biol, 19*(10), 1274-85.

Zitron IM, et al. (2013). Targeting and killing of glioblastoma with activated T cells armed with bispecific antibodies. *BMC Cancer, 13*(83).

APPENDIX

Specimen ID	Age/Gender	Diagnosis
BT241	68/F	R-GBM
BT428	63/M	P-GBM
BT458	81/M	P-GBM
BT459	60/M	P-GBM
BT624	59/F	P-GBM
BT698	57/F	P-GBM
BT799	77/M	P-GBM
BT935	53/F	P-GBM
BT993	52/F	P-GBM
NSC194	11w1d	Foetal NSPC
NSC195	13w4d	Foetal NSPC
NSC198	11w3d	Foetal NSPC
NSC200	13w1d	Foetal NSPC

Patient demographics. Recurrent GBM (R-GBM), primary GBM (P-GBM), neural stem and progenitor cells (NSPC). Gender was of the NSC specimens are not known. Age indicated by the number of weeks (w) and days (d)